Optimizing solar-assisted industrial heating and cooling system for cost-effective installation

Yacob Gebreyohannes Hiben[1, 2*], Mulu Bayray[1, 3], Johan Lauwaert[2]

[1]*Thermal and Energy Systems Chair, School of Mechanical and Industrial Engineering, Mekelle University, Endayesus Campus, P.O.Box 231, Mekelle, Ethiopia*

[2]*Department of Electronics and Information Systems, Faculty of Engineering and Architecture, Ghent University, iGent-tower, Technologiepark-Zwijnaarde 126, 9052 Ghent-Zwijnaarde, Belgium*

[3]*Department of Energy and Process Engineering, NTNU, 7491, Trondheim, Norway*

[*]Corresponding Author E-mail: yacob.gebreyohannes@mu.edu.et

Abstract

Integrating solar thermal collectors into industrial processes could be a viable way to replace the use of conventional fuels and achieve economic and environmental goals. However, there is a need to consider the detailed dynamic operation of a system with storage on a systematic control scale to fully optimize the realistic system performance under variable conditions by minimizing excess energy production and maximizing the annual life-cycle cost savings. In this study, we developed a TRNSYS-based dynamic statistical optimization model and evaluated FPC-based solar-assisted heating systems to achieve a cost-effective system design for two industries: MOHA soft drinks and Sheba leather factories in the Tigray region, Ethiopia. Three operating loads were compared: process heat, utility heat, and utility heat and chilled water. The optimized designs produced significant annual life-cycle cost savings, high solar fractions, and a good margin on temperature trends where the size of the solar collector has a greater impact. The annual cost savings per unit area of solar collector for process and utility heat was in the range of \$51-90/m^2 for collector mass flow and storage volume of 0.01-0.02m^3/h-m^2 and 0.04-0.08m^3/m^2, respectively. For utility heat and chilled water loads, the values were \$49/m^2 for a mass flow rate of 0.04m^3/h-m^2 and a storage volume of 0.07m^3/m^2. Thus, the study supports the transient analysis of solar-assisted industrial heat. The case studies have shown that the method provides optimal solutions for using solar thermal. As investment and financial sourcing remain a priority challenge, the model and case study results could help decision-making for similar and other production capacities, regions, industries, and solar technologies.

Keywords: *Solar thermal, Industry, Optimization, TRNSYS, Ethiopia*

Highlights

- Develops an economic optimization model for solar-assisted heat.
- Considers soft drink and leather processing industries in Ethiopia.
- Compares 3 load conditions with flexible heat integration.
- Optimized configurations solar fraction reached 99% for heating and 35% for cooling.
- Optimized configurations yielded annual cost savings of \$49-90/m^2.

Nomenclature

Abbreviations

ACH	Absorption Chiller

ALCC	Annual life-cycle cost
ALCS	Annual life-cycle savings
BB	Backup boiler
BC	Backup cooler
BCH	Backup chiller
BH	Backup heater
BR	Bottle rinse
BS	Bottle soak
CE	Collector efficiency
CHW	Chilled water
CHWD	Chilled water draw
CIP	Cleaning in place
COP	Coefficient of performance
CPC	Compound parabolic collector
CS	Crate soak
CSP	Concentrated solar power
CW	Cold water
DOE	Design of Experiment
ETC	Evacuated tube collector
FPC	Flat plate collector
HTF	Heat transfer fluid
HTN	Hide tanning
HRT	Hide re-tanning
HW	Hot water
HWR	Hot water return
LCOH	Levelized cost of heat
MATLAB	Matrix Laboratory
MSD	MOHA soft drinks
MW	Makeup water
PC	Production capacity
PHWD	Process hot water draw
PLC	Process level configuration
PTC	Parabolic trough collector
PWF	Present worth factor
RP	Radiation processor
RH	Running Hours
SC	Solar collector
SD	Sugar dissolving
SF_h	Solar fraction for heating
SF_c	Solar fraction for cooling
SHWD	Supply hot water draw
SIH	Solar-assisted industrial heat
SLC	Supply level configuration
SLI	Sheba leather industry
SO	Statistical optimization
SP	Solar pump
SRT	Skin re-tanning
SS	Solar system
ST	Storage tank
STN	Skin tanning
TRNSYS	TRNsient SYstem Simulation
UP	Uniform series of payments

Symbols

a_0	Intercepts efficiency with respect to aperture (%)
a_1	Slope heat loss coefficient (kJ/hm^2K)
a_2	Curvature heat loss coefficient (kJ/hm^2K)
b_1	First order incidence angle modifier
b_2	Second order incidence angle modifier
A_{SC}	SC area (m^2)
C_{ACH}	ACH controller

C_{ce}	Cost of conventional energy ($)
C_{CH}	Chiller cost ($/kW)
C_e	Electricity cost ($/kJ)
C_{es}	Cost of energy source ($)
C_f	Fuel cost ($/kJ)
C_{ins}	Installation cost ($)
C_{inv}	Investment cost ($)
C_{om}	Operation and maintenance cost ($)
C_p	Specific heat (kJ/kg^{0}C)
C_{SC}	Solar collector cost ($/m^2)
C_{SP}	Solar pump controller
C_{SS}	Solar system cost ($)
C_{ST}	Storage tank cost ($/m^3)
D_d	Daily demand
D_h	Hourly demand
d	Market discount rate (%)
E	Equation
E_{ann}	Annual energy consumption (GJ)
I_t	Total radiation on a surface (MJ)
i	Inflation rate (%)
M_C	Cold side mixer
M_H	Hot side mixer
m_{in_CW}	CW mass flow rate to ACH (kg/h)
m_{in_HW}	HW mass flow rate to ACH (kg/h)
m_{in_MW}	MW mass flow rate (kg/h)
m_{in_ST}	Mass flow rate to ST (kg/h)
m_{SC}	SC mass flow rate (kg/h)
N	System life (Years)
NC_{CH}	Chiller nominal capacity (kJ/h)
P	Process
Q_{ACH}	Heat removed by ACH (kJ/h)
Q_{BC}	Heat removed by BC (kJ/h)
Q_{BH}	Heat added by BH (kJ/h)
Q_{loss_ST}	Heat loss by ST (kJ/h)
Q_{ref}	Heat supplied form reference system (kJ/h)
Q_{SIH}	Heat supplied form SIH (kJ/h)
Q_{ST}	Heat added/removed in ST (kJ/h)
Q_u	Useful heat of SC (kJ/h)
T_{HWD}	HWD temperature (^{0}C)
T_{CHWD}	CHWD temperature (^{0}C)
T_{in_CW}	CW inlet temperature to ACH (^{0}C)
T_{in_HW}	HW inlet temperature to ACH (^{0}C)
T_{in_SC}	SC inlet temperature (^{0}C)
T_{low_db}	C_{SP} lower dead band temperature (^{0}C)
T_{MW}	MW temperature (^{0}C)
T_{out_BH}	BH outlet temperature (^{0}C)
T_{out_CW}	CW outlet temperature from ACH (^{0}C)
T_{out_CHW}	CHW outlet temperature (^{0}C)
T_{out_HW}	HW outlet temperature from ACH (^{0}C)
T_{out_SC}	SC outlet temperature (^{0}C)
T_{SC}	SC absorber temperature (^{0}C)
T_{set_ST}	ST set point temperature (^{0}C)
T_{top_ST}	ST top temperature (^{0}C)
T_{upp_db}	C_{SP} upper dead band temperature (^{0}C)
U	Utility
V	Valve
V_{ST}	Storage tank volume (m^3)
ρ	Density (kg/m^3)
η_{SC}	Instantaneous CE

1. Introduction

Conventional energy savings and low environmental impact are important elements for the conversion of the energy system to renewable energy sources. One way to replace conventional energy sources is to use SIH. In this work, SIH refers to different solar thermal technologies that absorb sunlight in the form of thermal energy and are combined with conventional utilities to transfer heat to an industrial process and provide a required heating load. The potential for the use of SIH systems is enormous in most countries around the world. Nevertheless, this potential is not exploited in many countries, especially in developing countries that suffer from energy shortages as social awareness of their potential and investment is generally limited [1]. SIH also has implementation issues, as solar energy is not stable for processes in industries that require on-demand energy [2]. The analysis presented in [3] also highlights the widespread use of low-cost coal as boiler fuel in South African industries, which poses a challenge to SIH deployment. However, companies using petroleum-based boiler fuels or electricity have a higher potential for savings if they adopt SIH. Therefore, the pursuit of continuous and optimal supply options based on least-cost planning can be considered as the backbone of this work, which in turn takes into account the diversification of the energy system and the associated high investment costs [4].

In recent years, the techno-economic and environmental viability of SIH plants has been studied in detail to achieve economic benefits, environmental benefits, or a mixture of both. For analysis of heat production, the characterization of solar radiation and producing industries is a starting point. This could help in understanding the solar potential and key industrial requirements. In practice, measured solar irradiance data is the most accurate but not always readily available, so a variety of models are used to estimate solar irradiance [5]. The amount and temperature level requirements in processing industries depend on the nature of the process. In addition, some processes have a continuous demand throughout the day, while others have a concentrated demand at certain times. The demand may vary daily, on certain days of the week, or throughout the months [6]. Thabit and Stark [7] studied the effects of work patterns on SIH in the United Kingdom and showed that low-temperature systems can provide 95% of the required thermal energy on clear and sunny days. Another condition that must be considered in the development of SIH is the choice of solar technology [8]. Primarily, solar technologies must be carefully selected to determine the best thermal performance. It should also be noted that 50 to 70% of the total system cost is attributed to the solar collector [9]. Kumar et al. [10] reported the results of a techno-economic analysis of their theoretical framework in the cotton-based textile industry for hot water and steam generation. It is found that SIH systems for hot water generation using FPC can be a good choice, while SIH systems for steam generation using PTC have longer payback periods and lower returns on investment. Experimental results by Garcia et al. [11] in the meat industry with large volumes at temperatures above 80^0C have shown that the deployment of solar hot water systems using ETC can be profitable in a wide range of locations and scenarios in Europe and that a return on investment (1.1€ per € invested) can be achieved and the heat supply can exceed 50% of the energy demand of almost 85000kWh/year. Among the techno-economic performance studies in Africa, a case study was conducted to investigate the technical and financial feasibility of a solar-powered industrial agro-processing system in Algiers [14]. Based on the connection type of the solar collector for which the economic feasibility study was carried out, an appropriate design of the system was determined by analyzing the LCOH savings. The design of the thermo-solar process was based on the F-chart method by integrating the incidence angle modifier using real and experimental data requirements to determine the realistic achievable performance of the solar process. The results show that the electrical energy savings achieved by the solar system are an economically viable option compared to the electrical system currently in use at a solar coverage rate of 80%. The investment depreciation balance shows that the use of such a solar thermal system is more competitive than a fossil fuel system when the electricity price in the country increases from 0.048 to 0.075€/kWh. In a case study of large-scale solar thermal systems in South Africa, 10 proposals for competitive bidding were compared in terms of cost, application, and benefiting industries. The proposed system installation costs varied by a factor of 2.5, indicating the low maturity of this market. The winning proposal has a gross collector area of 120.7 m^2, 7.9 €c/kWh LCOH, 16.7% IRR, and a payback period of 9.3 years [15].

In the past, few studies have been published that addressed SIH operation for variable temperature applications with maximum solar utilization. According to Porras-Prieto et al. [16], the energy performance and hot water extraction potential of a solar water heater with a heat pipe ETC, energy distribution and storage, control, and monitoring for different required temperatures (40^0C, 50^0C, 60^0C, 70^0C, and 80^0C) were experimentally studied. Essentially, this was the same system that is commercially available for water heating, with the difference that the control subsystem allows the water tank to be set at different temperatures. The results show that the net energy that can be stored by the device decreases as the temperature of the water tank increases. Another similar study by Mazarron et al. [17] investigates an experimental setup for a solar water heater with ETC in two scenarios: maximum profitability (100% usage) and assumption of a certain demand combined with diesel. In scenario 1, differences in net present value and a payback period of more than two years were obtained when going from 40°C to 80°C. However, the investment would pay off at any desired water temperature in the tank. In scenario 2, the analysis shows that the investment in the solar system can be profitably compared to a single system running on diesel, if the solar system is properly sized and the number of solar collectors is optimal, with a reduction in diesel consumption of almost 70% with a total annual irradiation in the collector plane of almost 2000 kWh/m^2.

Rather than maximizing solar utilization, SIH systems have also been studied by optimizing various design parameters to achieve economic benefits. In a study by Silva et al. [18], a thermo-economic design optimization of a PTC system was performed considering different economic objective functions to design an optimal system based on the annual thermal simulation performance of the system. They performed a multi-objective optimization routine to find the optimal trade-off between the payback period and life cycle savings. In Franco’s study [20], the design of a SIH plant was optimized using an approach that considers a synthetic combined energy and economic benefit function. The SIH plant was hybridized with natural gas and the solar fraction of the plant was maximized by up to 80% by optimizing the design with the proposed method. Among the optimization studies in Africa, the economics and optimal parameters of solar hot water systems for industrial processes in Alexandria, Egypt were investigated [12]. The industries covered were soft drinks and vegetable oil. Weather data for Alexandria, Egypt (31.2° latitude) were used. Economic calculations were based on ALCS. The F-chart method was used to estimate the long-term annual heat output of the system. The main results show that these systems are preferable to the conventional heating systems currently used in the Egyptian food industry and that significant ALCS can be achieved with solar heating systems. MATLAB-based mathematical modeling by Siyoum et al. [13], conducted for boiler feedwater heating in the beverage industry to provide heat at 85^0C using ETC in three cities in Ethiopia (average daily solar radiation of 4.7 to 7.6 kWh/m^2), showed significant fuel savings and CO_2 reduction potential of the system with optimized tilt angles of the collector. In the study by Allouhi et al. [19], an optimization process was carried out to size ETC to supply heat to four different processes at different temperatures, using a Moroccan milk processing plant as a case study. In this system, a stratified hot water tank was used to supply the four different processes at different temperatures. The analysis resulted in an optimized ETC area, tilt angle, and hot water storage volume to maximize ALCS. Overall, a comprehensive review of design optimization methods used for SIH systems can be found in [21].

From the literature reviewed, it appears that there is considerable research on optimizing SIH systems through more efficient operational and design considerations. However, there is a need to consider the detailed dynamic operation of a SIH system at a systematic control scale to fully optimize realistic system performance under variable conditions by minimizing excess energy production (maximizing solar utilization) and maximizing ALCS. Methods that take this approach can extend the findings from studies that use effective low-level control of flexible heat integration systems. This gap previously motivated a research work by Immonen et. al. [22], which focused on a heuristic operation optimization scheme for a PTC system. Using the developed optimization scheme, the control set points for the HTF outlet set point temperature and the amount of delivered heat split between two processes were continuously optimized to minimize the backup fuel consumption. This earlier study took a limited approach in that it did not consider ST, which may allow the system to contribute a larger solar fraction and ALCS while considering the overall system investment. It is clear that the addition of ST and the capital cost to improve storage management must be considered. Therefore, the current work is based on studies that perform economic optimization of SIH systems with ST considering ALCS. These previous studies led to the hypothesis that a SIH system with TS, which uses a systematic control scheme, can efficiently handle solar and load variations to provide heat in an economically optimal manner throughout the operating period. It is expected that optimized system performance and economics can be developed and studied through these optimization methods in conjunction with detailed dynamic operation and control. This will allow SIH systems to operate more economically and smoothly, and help eliminate the problems associated with using solar thermal for industrial heat.

Overall, the work in this study provides a new design process and methodology for the SIH system operation with ST to maximize ALCS. The methodology is based on a transient system analysis solved on a time scale of seconds to find optimal operating conditions and design parameters for a SIH system with flexible heat integration. A_{SC}, m_{SC}, and V_{ST} were the controlled design variables. The model controls SP with C_{SP} and simulates T_{SC} and T_{out_SC} by continuously monitoring $T_{top,\ ST}$. It incorporates accurate dynamic SO through a combination of adaptive DOEs to find optimal design parameters. Two factories, three operation cases, and two case study days were highlighted to show the trends of dynamic optimization solutions for different types of industries, integration points, and solar days. Finally, to illustrate the impact of design parameters, the sensitivity to the economic and thermal performance parameters was investigated by changing the design parameters.

2. Methods

In this section, the design of the SIH system proposed in this work for the integration of the process and utility levels is presented. First, the key system components and flow lines are presented. Then, the dynamic simulation, economic optimization, and thermal performance analysis methods are presented. Finally, data acquisition and processing for solar resources and industrial loads, as well as typical system performance values and economic parameters are summarized.

2.1. Physical structure and operation of the system

Figure 1 shows a schematic diagram of the proposed system, its components, flow lines, and control lines.

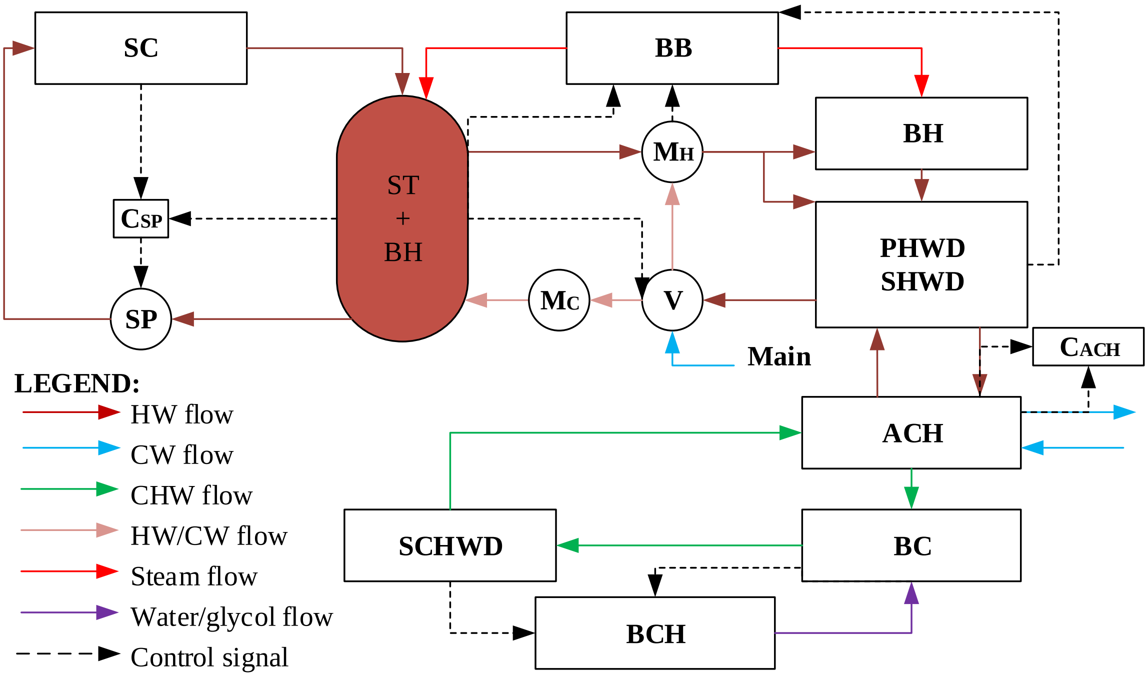

Figure 1: Proposed thermal energy and control signal flows for heating and cooling demands

In the proposed system, the main components of a solar system for PHWD, SHWD, and CHWD consist of SC, ST, BH, ACH, and BC. BH and BC are supplied by BB and BCH. In most cases, existing heating and cooling technologies in the industry were considered as BB and BCH rather than investing in new equipment to reduce the overall capital cost. These components are interconnected by piping and the flow in the various piping is controlled by actuating SP, V, M_C, and M_H.

Mass and control signal flows are involved to provide the required heating and cooling effects. These flows include the HW flow, the CW flow, the CHW flow, the steam flow, the water/glycol solution flow, the C_{SP} control signal, the BB control signal, the V control signal, the C_{ACH} control signal, and the BCH control signal. Three loops were considered: Solar loop, Heating load loop, and Cooling load loop. The solar circuit consists of SC, ST, internal BH, and SP. The heating load loop consists of ST, V, M_C, M_H, BH, PHWD, and SHWD. The cooling load loop is based on ACH, BC, and CHWD.

In the solar circuit, the amount of solar radiation received by SC is affected by I_t, A_{SC}, and the structure and material properties of the collector. The heat generated in SC is transported through the hydraulic circuit to ST. SP is turned on and off by a differential controller C_{SP}, which compares the measured temperatures T_{in_SC}, T_{out_SC}, and T_{top_ST} with the reference temperatures T_{upp_db}, T_{low_db}, and T_{set_ST}. The m_{SC} in the solar circuit depends mainly on A_{SC}, collector structure and material properties, and the properties of the HTF used in the system, such as ρ and Cp. SC, which is intended for hot water supply, usually uses water-based HTF; pure water is ideal (very cost-effective) for locations where freezing temperatures do not occur. When solar energy is sufficient to raise T_{top_ST}, the heat needed for industrial consumption is supplied by SC and the excess is stored in ST, represented by the positive heat swing ($+\Delta Q_{ST}$) until it reaches T_{set_ST}. From this point on, all the excess heat is dissipated. On the other hand, if the heat absorbed by SC is insufficient to meet the useful energy demand, the heat accumulated in the tank is used to make up this difference, which is represented by the negative heat variation ($-\Delta Q_{ST}$). In this case, to maintain the required T_{set_ST} or T_{HWD}, BB is activated and transfers Q_{BH} to the internal or external BH. This thermal inertia of the ST stabilizes the T_{out_ST} and simplifies the differential control for the circulation and the supply of the solar field.

In the load circuit, m_{in_MW} can flow directly to ST or can be partially or fully diverted to become m_{in_ST} based on a comparison between T_{HWD}, T_{MW}, and T_{top_ST}. This flexible heat exchange is fulfilled using V, M_C, and M_H. In this way, the storage delivers heat (Q_{SIH}) to the end users. For chilled water consumption, a differential controller C_{ACH} is used to activate ACH based on T_{in_HW} or T_{top_ST}, T_{out_CW}, and T_{out_CHW}. Thus, the chiller extracts heat ($-Q_{ACH}$) from the end users. The BCH extracts ($-Q_{BC}$) from the BC as needed and are based on T_{CHWD}.

2.2. Dynamic simulation and optimization

2.2.1. The simulation tool

TRNSYS [23] is one of the most popular simulation system programs with a complete and extensible simulation environment and modular structure for simulating systems with transient behaviour. The model design starts in “Simulation Studio” with the components available in the library, which are marked with the prefix “Type”. These are independent mathematical models (algebraic and differential equations) that can function both independently and in assembly. Based on the assembled components, the "Deck File", called the input text file, is created for the "Simulation Engine", which reads and processes the input file. The engine iteratively solves the system, determines convergence, and displays the system variables. The output managers are used to review the simulation results and fine-tune the simulation. They also generate a variety of user-defined reports on the simulation.

2.2.2. Model development and setup

Since the primary purpose of this analysis is to perform a dynamic simulation of the SIH system to analyze and optimize the effects of various input parameters on economic and thermal performance, the following simplifying assumptions are made in the TRNSYS modeling and simulation.

i. The system is assumed to be in equilibrium, which means that the temperature of the pipe and water is the same at every point, the mass flow rate is uniform, and no pressure losses are considered as no pressure relief valve is used.
ii. The effects of boiling the working fluid are not considered.
iii. Energy losses in the connected piping and valves are neglected.
iv. The thermal properties and heat capacity of the materials used remain the same and do not change with temperature.
v. There is no heat exchange between the components and the environment.

Next, two configurations based on the SIH system described in Figure 1 were investigated. The first (PLC) in Figure 2 is used to provide hot water for process heating. This configuration was a once-through system in which no hot water was returned to the storage tank from the processes. The hot water consumed was replaced by the main water supply based on the amount required by each of the six variable temperature processes shown. This scheme ensures that the storage tank is always fully charged.

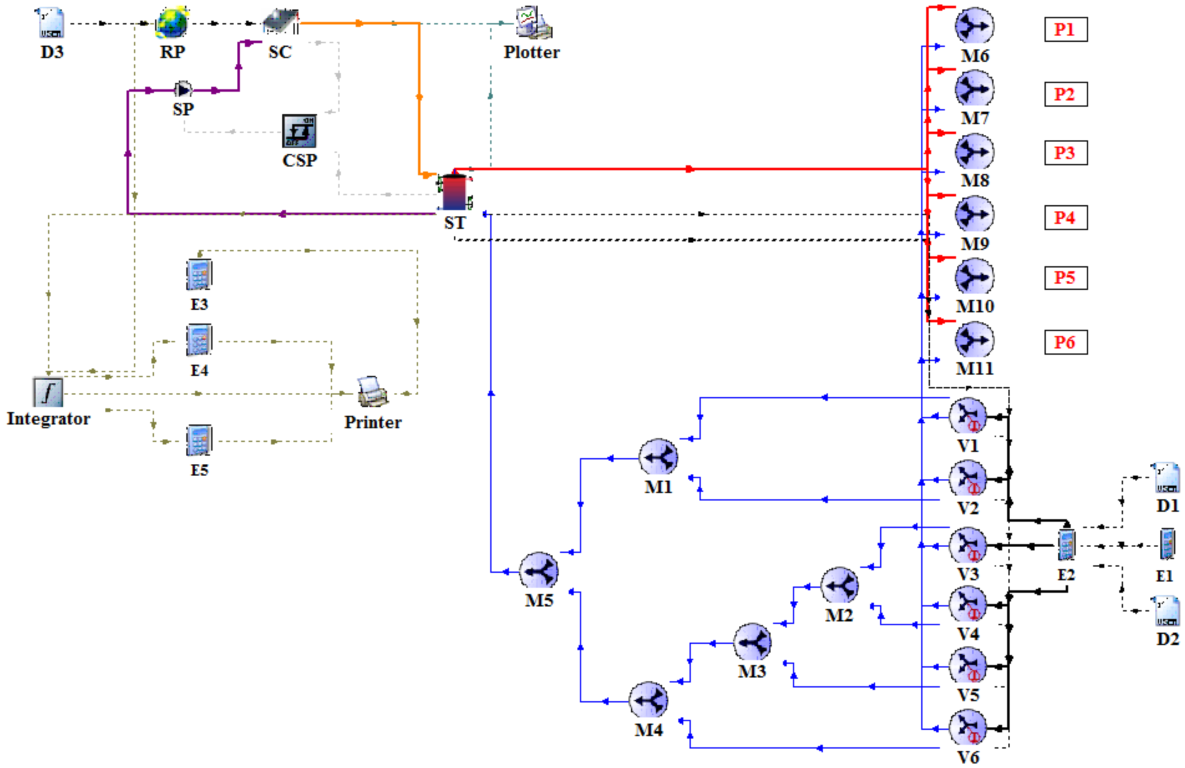

Figure 2: **PLC Solar-assisted heating system simulated in TRNSYS (with 6 processes)**

The second (SLC) is for preheating hot water to produce steam and chilled water. Figure 3 shows the model diagram for the SLC integration. This configuration was a closed system with steam condensates from the processes and hot water leaving the thermal cooling unit to return to the storage tank. Only the steam and hot water loss in the distribution streams was replaced by the main water supply. In the load circuit, the model was set to meet the heating demand first. In this scheme, the storage tank is not always fully charged.

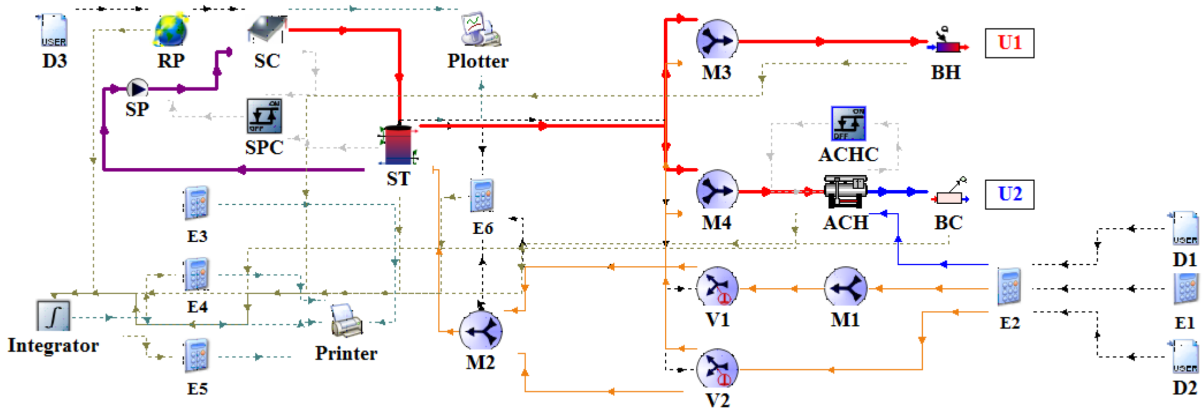

Figure 3: **SLC solar-assisted heating system simulated in TRNSYS**

Table 1 describes the TRNSYS component Types used in the models.

Table 1: **TRNSYS component Types description**

Component	TRNSYS Type	Function	Output
D1, D2, D3	Type 9	Reads user-defined horizontal radiation data (D3) and normalized thermal load of daily demand (D1) and weekly schedule (D2) for any industrial size.	Input data file
RP	Type 16	Calculates the radiation incident on a surface using horizontal radiation data and the tilt angle of the surface.	I_t

SC	Type 1	Extracts thermal energy from the incident radiation.	T_{SC} T_{out_SC} Q_u
ST	Type 4	Contains HTF circulating through the solar loop to store thermal energy and transfer it to the running processes as needed.	T_{top_ST} ΔQ_{ST}
P	Type 3	Circulates and maintains HTF flows based on external control.	m_{SC}
C1, C2	Type 2	Generates a differential on/off control signal depending on the upper and lower dead band temperature limits (T_{upp_db}, T_{low_db}) to regulate HTF flow rate and recirculation.	On/Off signal
V	Type 11	Redirects an inlet flow in the load loop based on internal control.	m_{in_ST}
M		Mixes two inlet flows of the load loop.	
BH	Type 6	Adds heat to the flow to increase temperature based on internal control.	T_{BH} Q_{BH}
ACH	Type 107	Extracts thermal energy from a stream of water through a single-effect, hot-water fired absorption chiller with normalized catalog data for any chiller size based on external control.	T_{ACH} Q_{ACH}
BC	Type 92	Extracts thermal energy from a stream to lower the temperature of a stream based on internal control.	T_{BC} Q_{BC}
E	Equation	Provides variable production capacity and temperature levels (E1) and variable design parameters (E3). Calculates load profile (E2), thermal performance (E4), costs (E5), and fraction of thermal energy to heating and cooling applications (E6).	Input data file CE, SF ALCS
Integrator	Type 24	Integrates a series of quantities over a period.	Weekly Annual
Printer	Type 25	Prints selected system variables at specified time intervals.	Results data
Plotter	Type 65	Displays selected system variables of the simulation.	Results plot

2.2.3. Dynamic simulation and optimization

The algorithm of TRNSYS software (version 17) allows the dynamic simulations to analyze the temperature and energy flow trends for the whole year, using a time step of 0.125h (450s). Search-based SO with genetic algorithms using DOEs evaluates the design space and makes predictions about promising regions [24]. The simulations required to obtain optimal results were constrained by three decision variables (A_{SC}, m_{SC}, and V_{ST}) with defined upper and lower bounds to limit the decision variable space. These sets of decision variables were generated based on the annual, daily, and hourly industrial demand and solar radiation potential of the study area. The mathematical equations are listed in Table 2 [25].

Table 2: A_{SC}, m_{SC}, and V_{ST} equations and bounds

Equation	Upper and lower bounds
$A_{SC}(\mathrm{m}^2) = \dfrac{\sum_{annual} m_{in\_ST} Cp\Delta T_{HWD}\ (kJ)}{CE \sum_{annual} I_t}$	$0 < \mathrm{m}_{in\_ST} < \mathrm{m}_{main}$
$m_{SC}(\mathrm{kg/h}) = \dfrac{A_{SC} \sum_{hour} I_t\ \ (kJ)}{C_p \Delta T_{SC}}$	$0 < \sum_{hour} I_t < \left(\sum_{hour} I_t\right)_{max}$
$V_{ST}(\mathrm{m}^3) = \dfrac{A_{ST} \sum_{day} I_t - \sum_{day} m_{in\_ST} Cp\Delta T_{HWD}\ \ (kJ)}{\rho Cp \Delta T_{ST}}$	$0 < \mathrm{m}_{in\_ST} < \mathrm{m}_{main}$

To formulate the space of decision variables, 5 values within its upper and lower bounds were considered for each decision parameter. From these sets, preliminary variables were used to start the analyses, and these values were changed until the termination criterion was met (125 annual dynamic simulation runs for the different combinations of the 5 data points). The flowchart of the TRNSYS analysis procedures is shown in Figure 4.

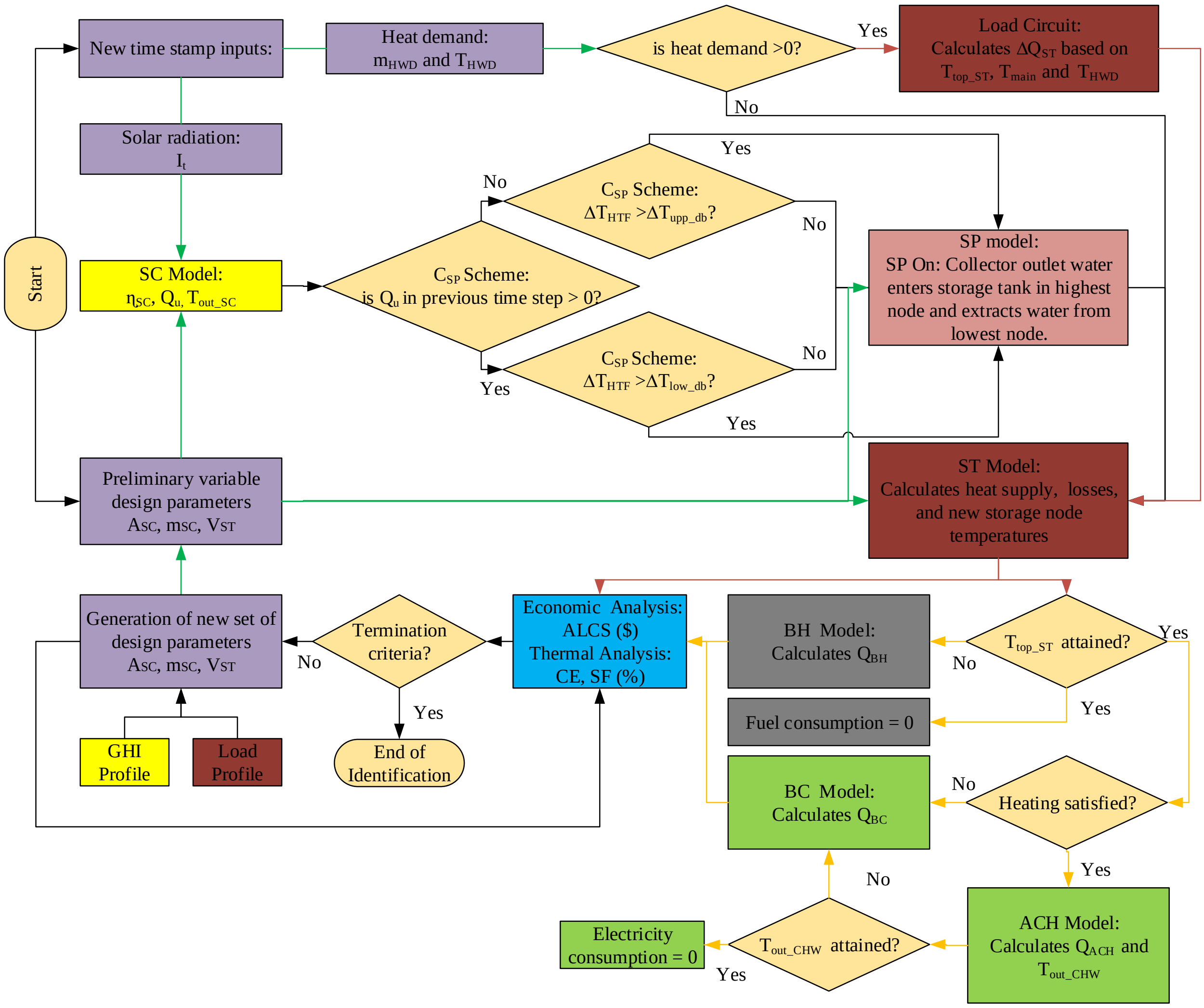

Figure 4: TRNSYS model simulation and parameter identification/optimization block

For each calculation, the solar radiation and heat demand timestamps were read from the input files. The SC model calculates the values η_{SC}, Q_U, and T_{out_SC}. The Pump turns on/off according to the T_{upp_db} and T_{low_db}. The consumption circuit draws heat (ΔQ_{ST}) from the ST based on T_{top_ST}, T_{HWD}, and T_{MW}. The ST model calculates the Q_{ST}, Q_{loss_ST}, and the new temperatures of the storage nodes according to the ΔQ_{ST} and the ambient conditions. If the new storage temperature reaches the set value, no fuel consumption is required; otherwise, the BH model calculates the amount of heat to reach the required temperature (Q_{BH}). When the new storage temperature reaches the set value, the ACH model also calculates Q_{ACH} and T_{out_CHW}. When the chilled water temperature reaches the T_{out_CHWD} set point, no electricity consumption is required; otherwise, the BC model calculates the amount of energy needed to meet the demand (Q_{BC}). The total delivered energy was calculated from the ST, BH, and BC models for the calculation of cost savings (ALCS) and thermal rating (CE, SF). Once the calculations were complete, area plots of the results were generated to identify promising regions.

2.3. Defining the optimization model

For each main component of the system (SC, ST, and ACH), the initial cost and the percentage of capital cost for their installation and maintenance have been determined. The cost of each component depends mainly on its size. The mathematical expressions were based on a series of payments, from which the cost estimation was performed to evaluate the ALCC of the system using the equations in Table 3. The economic criterion was described in detail by Duffie and Beckman [23].

Table 3: Equations of economic indicators

Indicator	Formula
ALCC of reference system	$ALCC_{ref} = C_{ce}(UP)(PWF)$
First year conventional energy cost	$C_{ce} = E_{ann}C_{es}$
Uniform series of payments or annual cash flows	$UP = \frac{d*(1+d)^N}{(1+d)^N - 1}$
Series of inflating payments or present worth factor	$PWF = \frac{1}{(d-i)}\left[1 - \left(\frac{(1+i)}{(1+d)}\right)^N\right]$
ALCC of SIH system	$ALCC_{SIH} = C_{inv} + C_{ins} + C_{om} + C_{ce}(UP)(PWF)$
Investment cost	$C_{inv} = A_{SC}C_{SC} + V_{ST}C_{ST} + NC_{CH}C_{CH}$
Installation cost	$C_{ins} = \%C_{inv}(C_{inv})$
Maintenance cost	$C_{om} = \%C_{SS}(A_{SC}C_{SC} + V_{ST}C_{ST} + C_{acc})$

The objective function was defined by the annual life cycle savings (ALCS) in Equation (1):

Objective function $$Maximize\ (ALCS = ALCC_{ref} - ALCC_{SIH}) \quad (1)$$

Based on the description in the previous section, linear temperature constraints were assumed (Table 4). These constraints aim to limit the operating parameters important to the thermal model, including ensuring heat transfer based on temperature differences to minimize excess energy production.

Table 4: System control strategy and values

Component	Constraints	Remark
SP	On: $T_{out\_SC} - T_{in\_SC} > T_{upp\_db}$ and $T_{top\_ST} < T_{set\_ST}$ Off: $T_{out\_SC} - T_{in\_SC} < T_{low\_db}$ and $T_{top\_ST} > T_{set\_ST}$	$T_{set\_ST} = (T_{HWD})_{max} + 10^0c$ $T_{set\_top\_ST} = (T_{HWD})_{max}$
V	$m_{in\_ST} = m_{MW}$: $T_{MW} < T_{top\_ST} < T_{HWD}$ $m_{in\_ST} = (T_{HWD} - T_{MW} / T_{top\_ST} - T_{MW})\ m_{MW}$: $T_{MW} < T_{HWD} < T_{top\_ST}$	
ACH	Stop: $T_{out\_CHW} \leq T_{CHWD}$, $T_{in\_HW} < T_{ACH\_HW}$, $T_{out\_CW} > T_{ACH\_CW}$	
BH	Stop: $T_{top\_ST} \geq T_{set\_top\_ST}$ (Internal), $T_{BH} \geq T_{HWD}$ (External)	
BC	Stop: $T_{out\_CHW} \leq T_{CHWD}$	

2.4. Defining the thermal performance

To compare the SIH system on an energetic basis, the matrices CE and SF were used. Thus, CE, defined by the ratio between the energy received and the energy captured, can be estimated by Equation (2):

$$CE = \frac{Q_u}{A_{SC}I_t} \quad (2)$$

SF is defined by the percentage of the total thermal load provided by solar energy. It is estimated by Equation (3) for heating and Equation (4) for cooling.

$$SF_h = 1 - \frac{Q_{BH}}{(Q_u + Q_{BH}) - \left(Q_{ACH}/COP_{ACH}\right)} \quad (3)$$

$$SF_c = 1 - \frac{Q_{BC}}{Q_{ACH} + Q_{BC}} \quad (4)$$

2.5. Case study selection and overview

This step includes the collection of solar radiation and industrial production data, formulation of energy and mass balances, and development of solar resource and load profiles. The selection of case study locations and industrial facilities is mainly based on climatic conditions, solar irradiance, and the presence of industrial facilities. Based on the established criteria, a case study was conducted in MSD and SLI in Ethiopia in the Tigray region. The mean daily horizontal irradiance in Ethiopia is higher than 5kWh/m^2-day. Seasonally, the values vary between 4.55 and 5.55kWh/m^2-day and spatially between 4.25kWh/m^2-day and 6.25kWh/m^2-day [26][27][28]. The manufacturing sector in Ethiopia is characterized by a high concentration of a limited number of light manufacturing activities, such as food and beverages, leather, textiles, non-metallic materials, and furniture [29]. The main processes of these industries require low- to medium-temperature hot water and low to medium-capacity process cooling.

2.5.1. Solar resources

Since few solar irradiance data are available, a validated correlation was developed based on measurements in the Geba catchment area in northern Ethiopia to predict the intensity of solar irradiance and determine the optimal orientation [30]. The horizontal solar irradiance was converted to a plane at optimal angles of incidence of 15^0 for the MSD case and 25^0 for the SLI case. A file of solar radiation data was generated in a user-defined format for the locations of the selected industries. The average hourly solar irradiance reached a maximum value of 1100W/m^2. The total annual surface irradiation was approximately 2400kWh/m^2.

2.5.2. Process and utility loads

The PC of MSD is 3600 bottles/h (150 cases/h). The production processes run in two shifts 6 working days per week, excluding holidays, machine downtime, and planned maintenance, resulting in an average annual availability of 82.60% (258 days/year). The manufacturing processes include SD, BS_1, BS_2, BR, CS, and CIP. In SD, sugar is dissolved in HW in three batches for preparing simple syrup. This syrup is continuously cooled with chilled water as it flows into the final syrup tank. The final syrup (soda) is also cooled as it flows to the bottle filler. In BS_1, BS_2, BR, and CS, bottles and crates are continuously washed in a series of tanks before filling. HW is used for the washing process. In the CIP, HW is used to clean the lines and tanks in the manufacturing processes according to the changeover matrix.

SLI's PC is 6000 skins/day and 600 hides/day. The production processes run in two shifts, alternating 6 and 5 working days every two weeks. No work is done during holidays, machine downtime, and scheduled maintenance, resulting in an average annual availability of 94.84% (272 days/year). The wet-blue processes include STN, HTN, SRT_1, SRT_2, HRT_1, and HRT_2 in different drums with different volumes using HW prepared in a separate tank.

The HW demand in MSD and SLI is met by superheated steam from a fuel-based boiler in place (T ≈ 100-190°C, efficiency ≈ 80%, and capacity ≈ 4000kg/h). The CHW demand in MSD is met by an electrically driven ammonia-based chiller in place (T ≈ 0°C, COP ≈ 4.4, capacity = 396kW).

The MSD and SLI systems analyzed are modeled as a retrofit problem. A flowchart of their PLC and SLC modeling is shown in Figure 5.

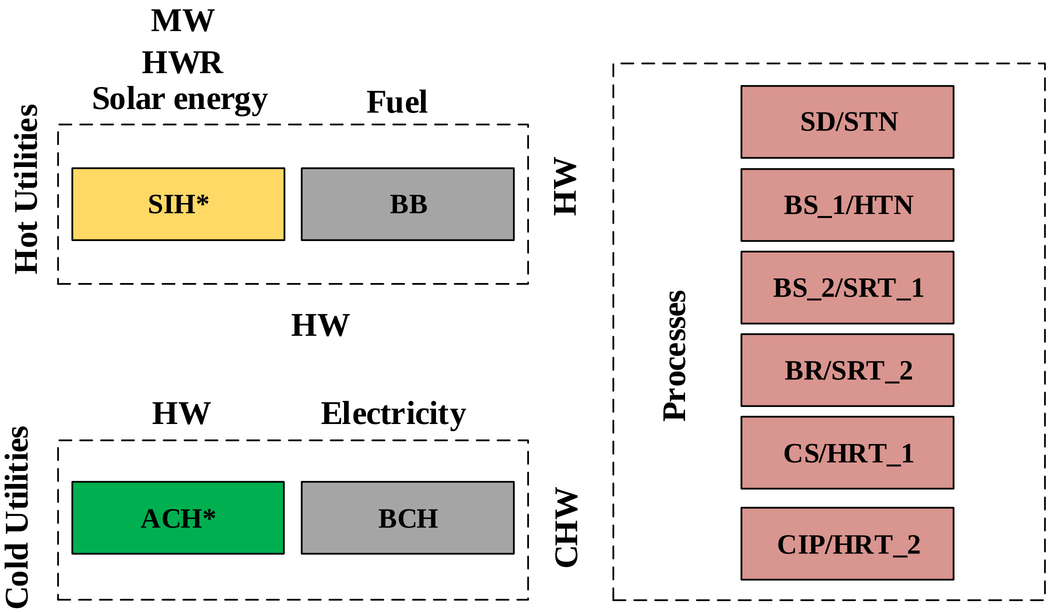

Figure 5: Flowchart of PLC and SLC in MSD and SLI (units with * are newly added)

Process HW demand is met by heating MW (≈20^{0}C). Utility HW demand is met from the condensate HWR (≈70^{0}C), chiller HWR, and MW (≈20^{0}C) to offset water losses to the processes. All or a portion of these streams flow through the SIH system, depending on the control temperatures. A solar fraction can be as high as 100%, but depending on the availability of solar energy, this fraction can be reduced. When the solar fraction is less than 100%, the HW demand is met by superheated steam from the existing fuel-based BB and CHW demand is met by an electrically powered ammonia-based BCH on site.

For the proposed flowchart, primary data collection was conducted using installed instrumentation. Secondary data were collected from existing records, monthly energy and fuel bills, process manuals, and machine catalogs available in MSD and SLI and in the literature. The heat load profiles of the processes included in the analysis are shown in Table 5.

Table 5: Processes load profile

Industry	Unit Operation	D_d (m^3)	T_{MW} / T_{HWR} (^{0}C)	T_{HWD} (^{0}C)	RH
MSD	SD	27	20	80	7AM to 8AM 11AM to 12PM 4PM to 5PM
	BS_1 BS_2 BR CS	68 51 10 70	20	75 80 60 40	7 AM and 7 PM
	CIP	20	80	85	8PM to 9PM
SLI	ST HT SRT_1 SRT_2 HRT_1 HRT_2	24 21 23 10 18 6	20	35 40 40 50 45 55	1PM to 5PM 1PM to 3PM 7AM to 10AM 4PM to 5PM 11AM to 12AM 11PM to 12PM

MSD and SLI operate mainly during daytime hours from 6:00 am to 6:00 pm. In MSD, there is an almost uniform continuous demand with evenly distributed batch demands, resulting in an even distribution of pick demand in the morning, noon, afternoon, and evening. In SLI, there is a discontinuous (batch) load profile with a pick demand for hot water around midday.

The hot and cold utility load profiles are listed in Table 6.

Table 6: Utilities load profile

Industry	Stream	D_d (m^3)	T_{MW} / T_{HWR} (^{0}C)	T_{HWD}/T_{CHWD}(^{0}C)	RH
MSD	CS MW	41 1	70 20	85	7AM to 9PM
	CHW	650	11	4	7AM to 7PM
SLI	CS MW	10 15	70 20	80	7AM to 6PM

In both processing industries, there is a constant supply of preheated feedwater as part of steam generation during working hours. In MSD, much of the feedwater comes from CS. In SLI, a similar proportion of CS and MW are reported as feedwater. This CS is used directly to produce hot water for the skin tanning process. In addition, in MSD, a constant supply of CHW is identified as part of the utility services.

Data from the plants on the amount of HW consumed daily and the amount of steam and CHW produced were used to model the load profiles. Equation (5) was employed to normalize the hourly load profiles based on D_d, RH, and PC. The details of the process load study can be found in the authors' earlier work [31].

$$D_h = \frac{\left({}^{D_d}/_{RH}\right)}{PC} \tag{5}$$

A HW and CHW demand file was developed in a user-defined format for the following operating loads to serve multiple users in the load balancing approach.

- Load 1: Process heat loads.
- Load 2: Feedwater preheat load.
- Load 3: Feedwater preheat and chilled water loads.

MSD HW demand reaches about 54.30 GJ and 3.6 GJ per day for Load 1 and Load 2, respectively. In addition, HW and CHW demand reaches about 23.80 GJ and 23.76 GJ per day for Load 3. SLI HW demand reaches about 11.60 GJ and 5.32 GJ per day for Load 1 and Load 2, respectively.

2.5.3. FPC system

The water-based single-glazed FPC is modeled using available performance data. The operating temperature range is matched to the process demand and ranges from 35 to 85^{0}C. To replicate an accurate FPC system, the typical performance and economic parameter values in Table 7 and Table 8 were used from various literature, component technical documentation, and existing systems. Several parameters can be easily changed in various ways to meet the required application.

Table 7: Typical solar thermal components performance parameters

Component	Parameter and Unit	Value

FPC [32][33][34]	a_0, % a_1, kJ/ h m²K a_2, kJ/hm²K² b_1 and b_2	0.8 13 0.05 0.2 and 0
HTF [32]	C_P, kJ/kg K ρ, kg/m³ Boiling point, ⁰C	4.19 1000 100
C_{SP} [23]	T_{upp_db}, ⁰C T_{low_db}, ⁰C	4 2
ST [35][36]	Loss coefficient, kJ/h m² K Height, m Maximum internal heating rate, kJ/h Dead band for heating element delta, ⁰C	2.5 2.8 10000000 5
ACH [34][37][38]	NC_{ACH}, kJ/h COP m_{in_HW}, kg/h T_{in_HW}, ⁰C T_{out_HW}, ⁰C m_{in_CW}, kg/h T_{in_CW}, ⁰C T_{out_CW},⁰C	1368000 0.76 42,000 88–98 78–88 102,000 28 36

Table 8: Typical solar thermal and backup system components economic parameters

Component	Parameter and Unit	Value
SS [35][39][40]	C_{SC}, \$/m² C_{ST}, \$/m³ C_{ins}, (% C_{inv}) C_{om}, (% C_{SS}) N, Years	200 1320 1 1.5 20
ACH [37]	C_{ACH}, \$/kW N, Years	657 60
BB and BCH [41][42]	C_f, \$/kJ C_e, \$/kJ	0.00002 0.0000056
Market values [43][44]	i, % d, %	9.4 10

3. Results and Discussion

Optimization of system parameters was performed using the model and procedures described in the previous section. The decision variables were those associated with the size of A_{SC} and V_{ST}, and the amount of m_{SC} that maximizes ALCS during 20 years of energy cost and investment. The optimized sizing of SIH systems was based on solar irradiance and the three load types adopted in MSD and SLI in Ethiopia. In this section, the results of the optimization analysis are presented to demonstrate the achievable benefits of the SIH system using the upper and lower bounds of the decision variable space for the main design parameters as shown in Table 9.

Table 9: Design parameter bounds

Industry	Thermal load	A_{SC} (x100 m²)	m_{SC} (m³/h)	V_{ST} (m³)
MSD	Load 1 Load 2 Load 3	10-110 1.50-7.50 3-11	3-465 0.6-35 5-750	70-350 5-45 20-100
SLI	Load 1 Load 2	2.25-15.75 1.25-7.50	1-105 0.4-26	20-100 10-50

The ALCS maps of the studied cases that are close to the optimal solution for the maximum achieved ALCS are presented in area plots. The ALCS varies with the values of the design parameters, the radiation intensity, and the different load profiles. This led to an optimal design of the system for each integration point and for each industry. In the MSD, Load 1 (Figure 6) resulted in the largest design parameters and ALCS values, while Load 2 (Figure 7) resulted in a relatively lower value.

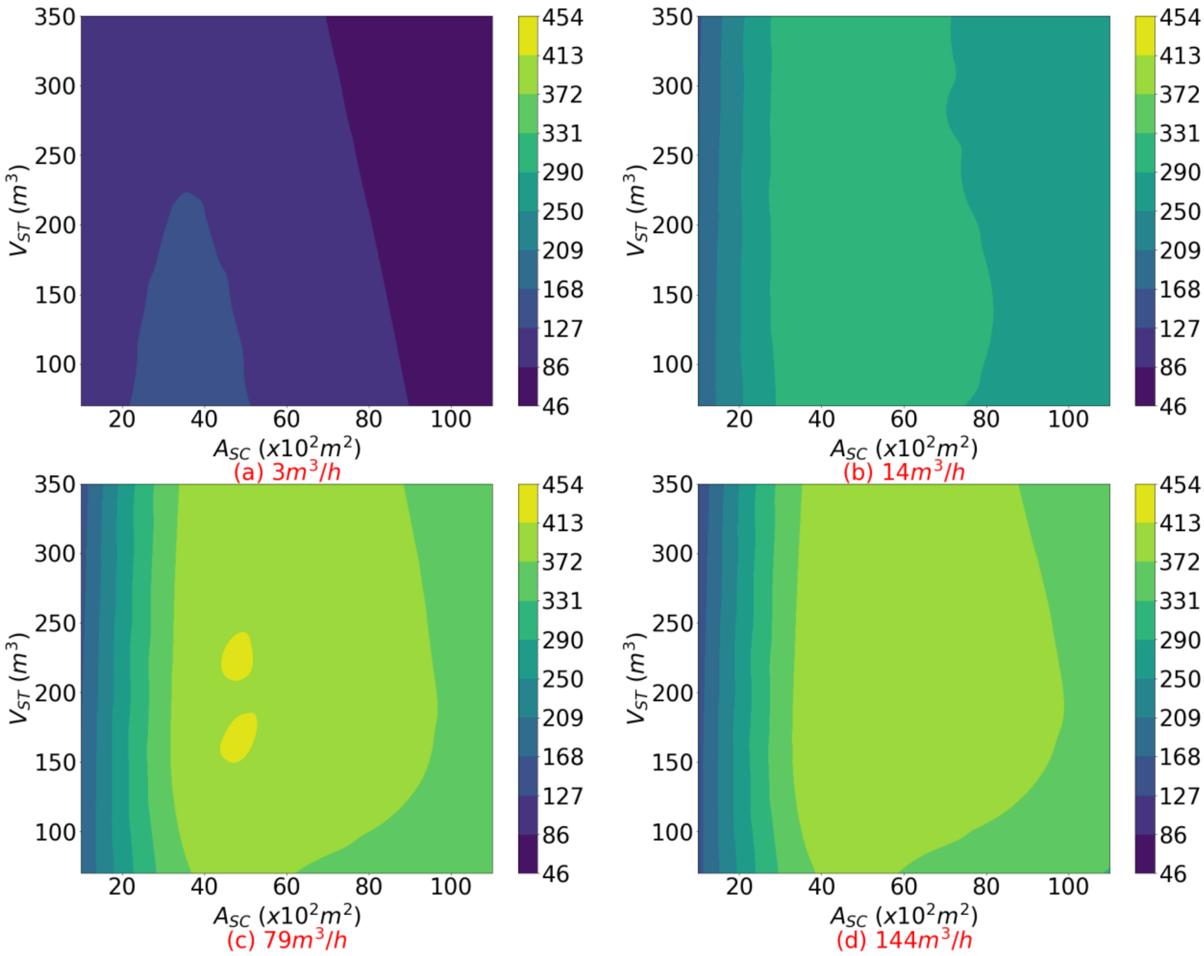

Figure 6: **ALCS (k$) results of TRNSYS model for MSD Load 1**

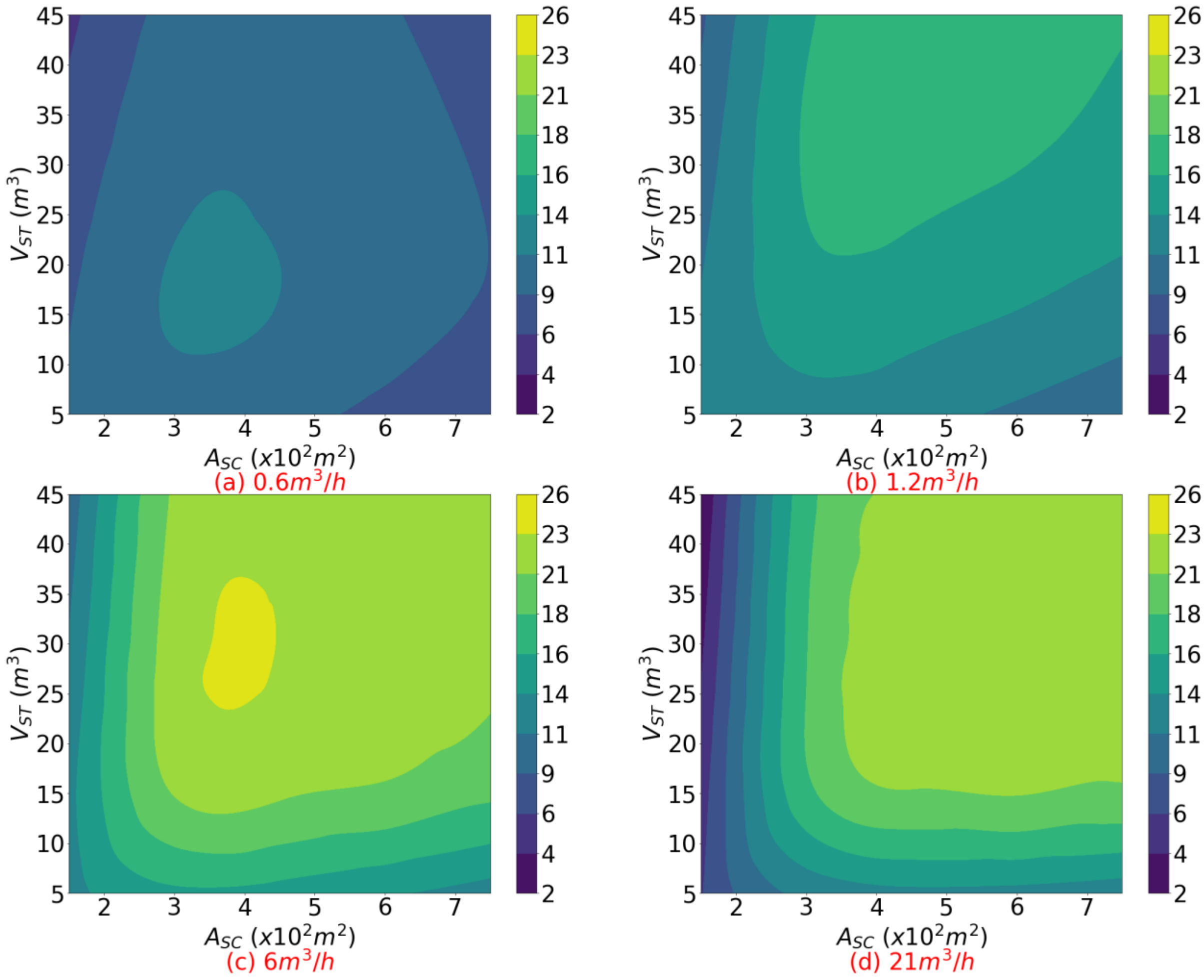

Figure 7: ALCS (k$) results of TRNSYS model for MSD Load 2

MSD Load 3 (Figure 8) was a less costly operating scheme with the highest ALCS values and design parameters compared to Load 2 (Figure 7). This may be attributed to the fact that replacement with solar thermal collectors may be less practical at higher supply temperatures and relatively low collector mass flow.

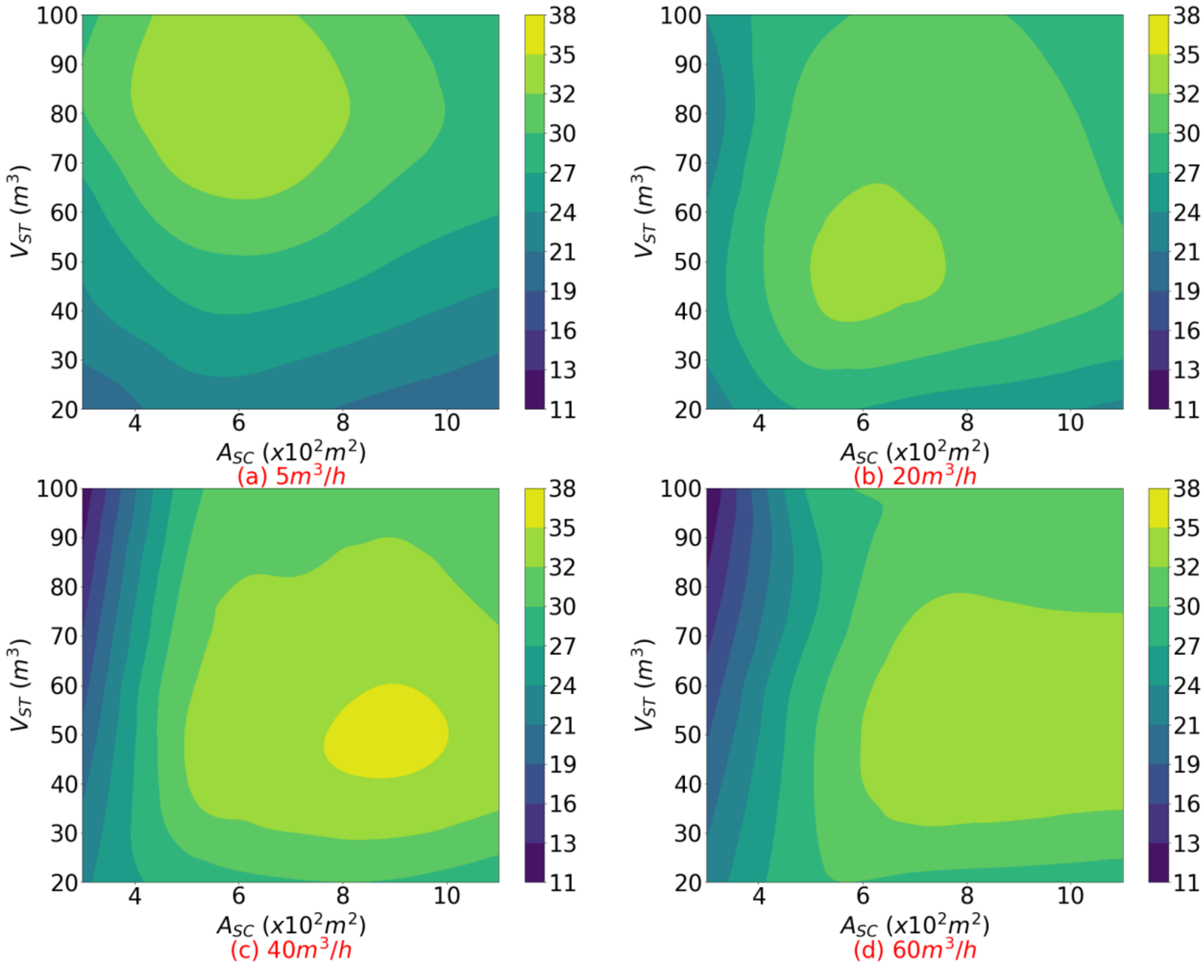

Figure 8: ALCS (k$) results of TRNSYS model for MSD Load 3

Similarly, SLI resulted in large design parameters and ALCS values for Load 1 (Figure 9), while Load 2 (Figure 10) resulted in relatively low values.

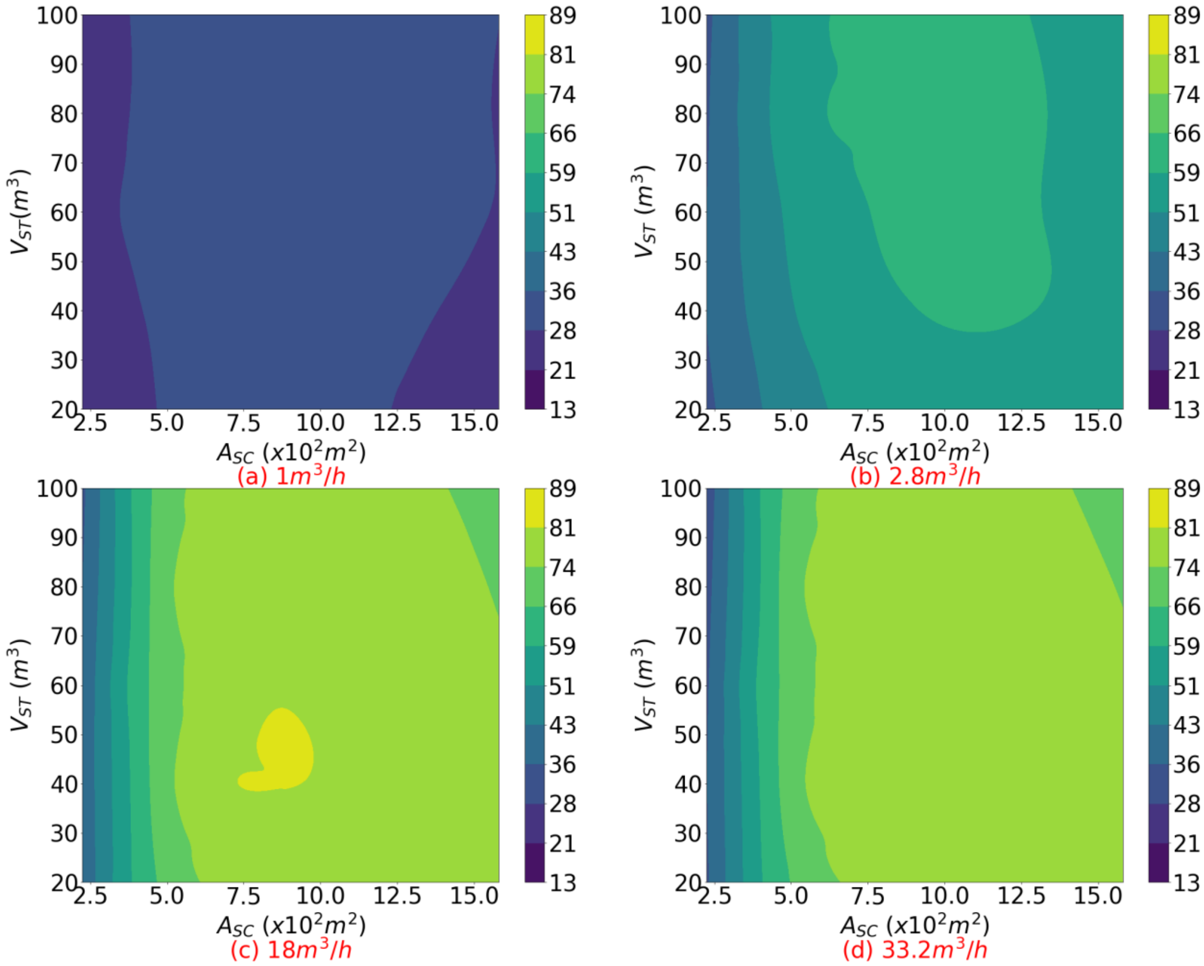

Figure 9: ALCS (k$) results of TRNSYS model for SL Load 1

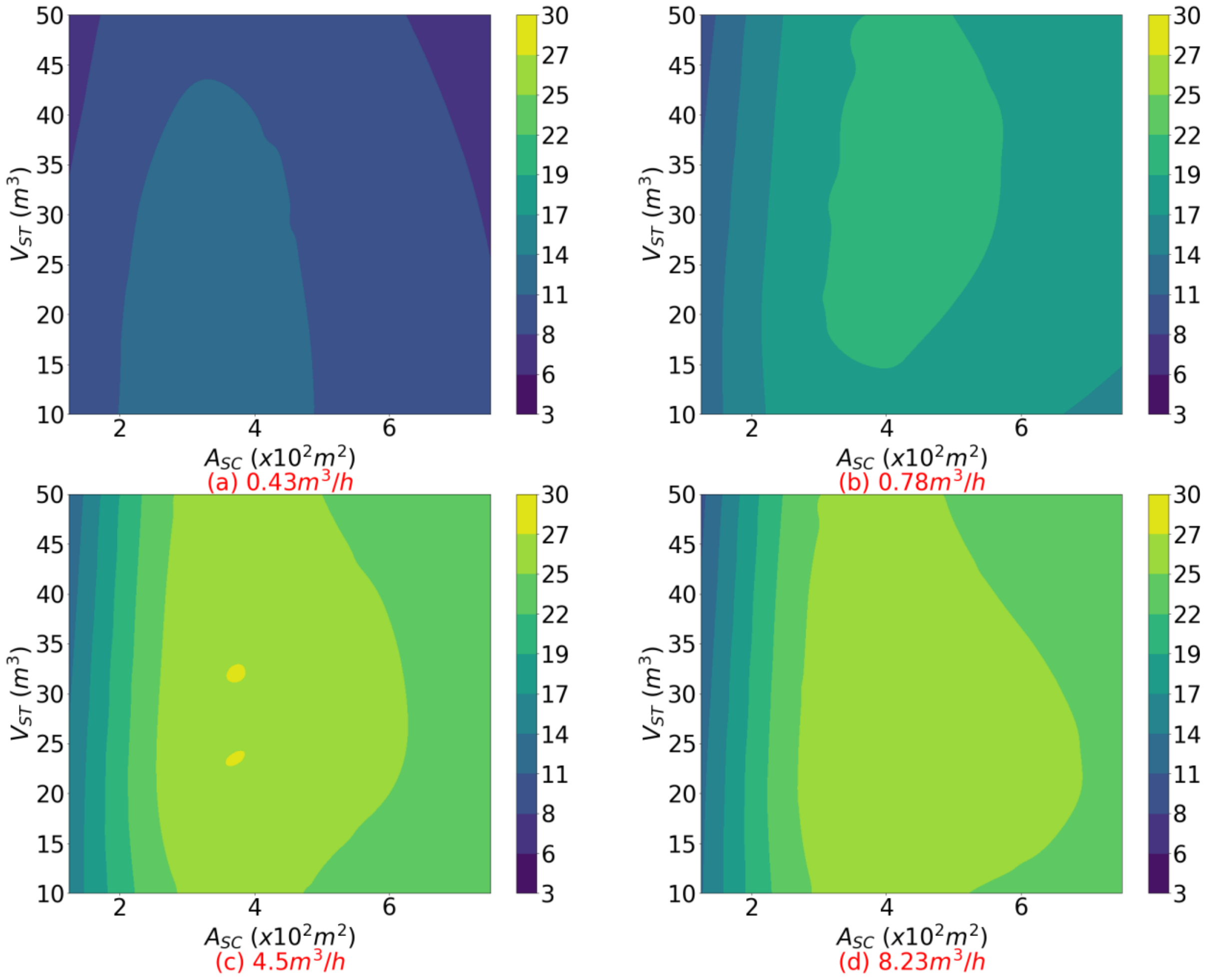

Figure 10: ALCS (k$) results of TRNSYS model for SL Load 2

A summary of the design parameters and performance values for the optimized configurations can be found in Table 10.

Table 10: Design parameter and performance values of the optimized configurations

Industry	Thermal load	Maximum ALCS (k$)	A_{SC} (x100 m^2)	m_{SC} (m^3/h)	V_{ST} (m^3)	CE (%)	SFh/SFc (%)
MSD	Load 1	403	60	79	210	27	98
	Load 2	23	4.5	6	35	24	94
	Load 3	35	9	40	60	29	96/19
SLI	Load 1	81	9	18	40	34	98
	Load 2	26	5	8	20	22	97

A positive ALCS value indicates the cost-effectiveness of a system over its lifetime. In comparison, Load 1 in MSD with a larger collector area and storage volume achieves the highest ALCS value. In contrast, Load 2 in SLI achieves a higher ALCS with a smaller storage volume and a slightly larger collector area. In MSD Load 3, the additional cooling load of the utility system gives the solar system an advantage and results in a high ALCS value.

The higher the value for CE and SF, the more solar thermal energy can be obtained with the technologies used. Overall, the thermal performance was higher for Load 1 due to the low supply temperature and even better for SLI due to the low target temperatures. Load 2 had a comparable performance at similar target temperatures in the MSD and SLI utilities. The thermal performance was improved at Load 3 primarily due to the higher mass flow rate of the collector to meet the HW demand of the large volume of CHW. These results are consistent with those reported in [7] that solar energy-based low- and medium-temperature systems can provide 95% of the required thermal energy on clear and sunny days.

3.1. Thermal evaluation

The analysis of the one-day performance of the solar circuit in the two seasons of the study area was able to show the trend of collector temperatures, storage temperature, useful energy yield, and supplementary heating demand for the studied cases. On a daily basis, it was observed that the collector starts to heat up from around 7 am, reaches the highest temperature around 12 noon, and drops again around 6 pm.

In the MSD, a maximum T_{SC} of 160^0C can be reached during the dry season for Load 1 (Figure 11a) and Load 2 (Figure 12a) in the dry season. This often occurred during stagnation conditions. The maximum T_{out_SC} of Load 1 (Figure 11b) and Load 2 (Figure 12b) reached 85^0C during the rainy season. During the dry season, there may be an excess of solar thermal generation at the peak solar hours for Load 1 and Load 2 (Figures 11c, 12c). The potential contribution of solar thermal generation can be insufficient during the morning and evening hours of the rainy season for Load 1 and Load 2 (Figures 11d, 12d) and during the morning hours of the dry season for Load 2 (Figure 12c).

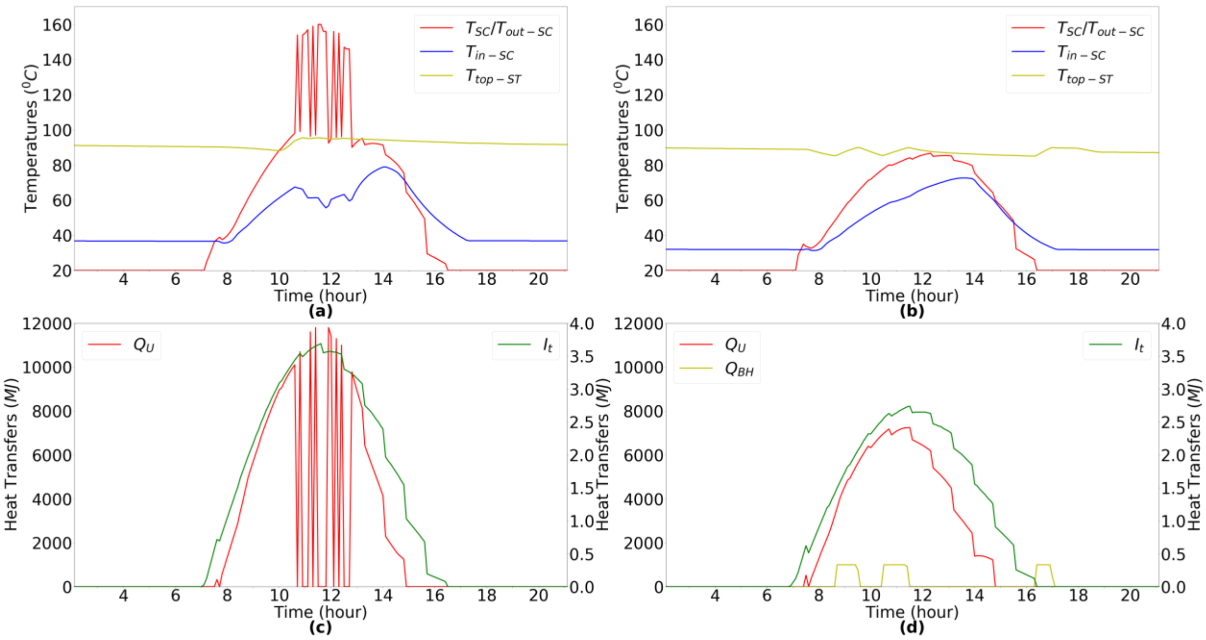

Figure 11: Performance of PLC TRNSYS model in MSD Load 1 (a)&(c) dry, (b)&(d) rainy season

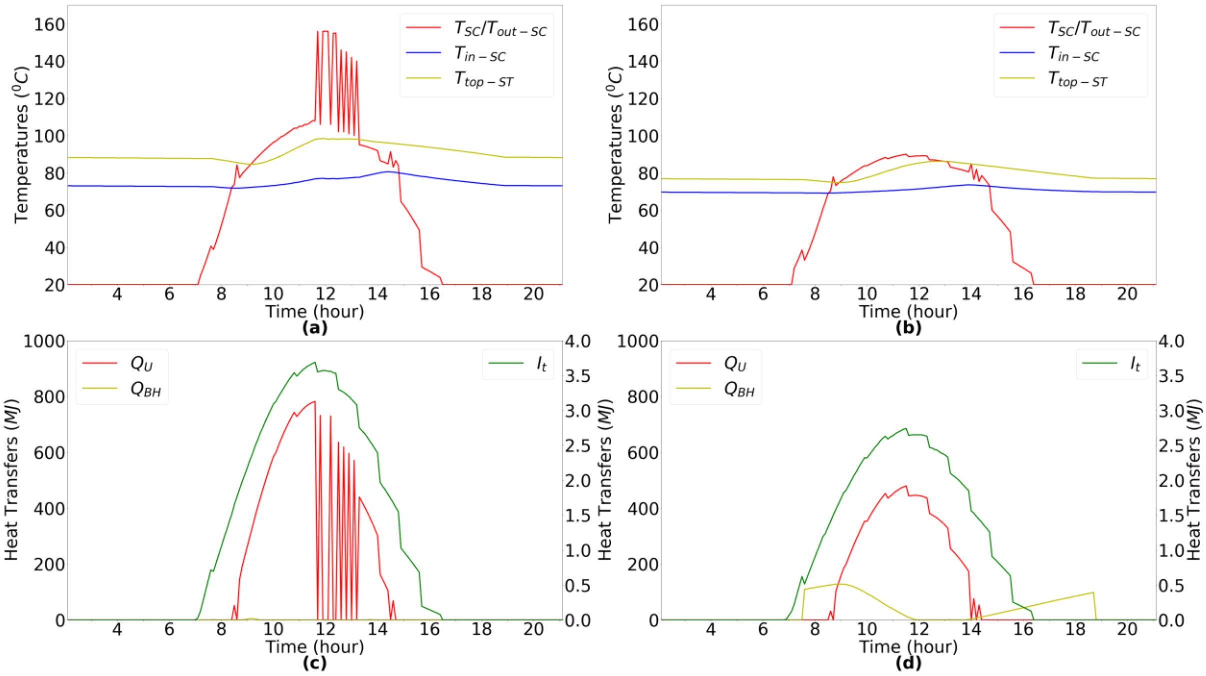

Figure 12: Performance of SLC TRNSYS model in MSD Load 2 (a)&(c) dry, (b)&(d) rainy season

A maximum T_{SC} of 120^0C can be achieved in the dry and rainy seasons under stagnant conditions for Load 3 (Figures 13 a, b). T_{out_SC} around noon reaches 85^0C as a result of higher mass flow during the hours of higher solar radiation to provide hot water for the thermal chiller, resulting in continuous cooling of the collectors and thus better performance of the FPC (Table 10). Figure 13c shows that there may be a shortage of solar thermal generation for cooling purposes during the dry season in the morning and evening hours, while the potential contribution of solar thermal for cooling remains insufficient at additional times during the rainy season (Figure 13d). This is because thermal energy only needs to be provided for heating needs until sufficient thermal energy has been generated for the thermal chiller, resulting in excess solar thermal generation during the morning and evening hours even for the optimal system configurations.

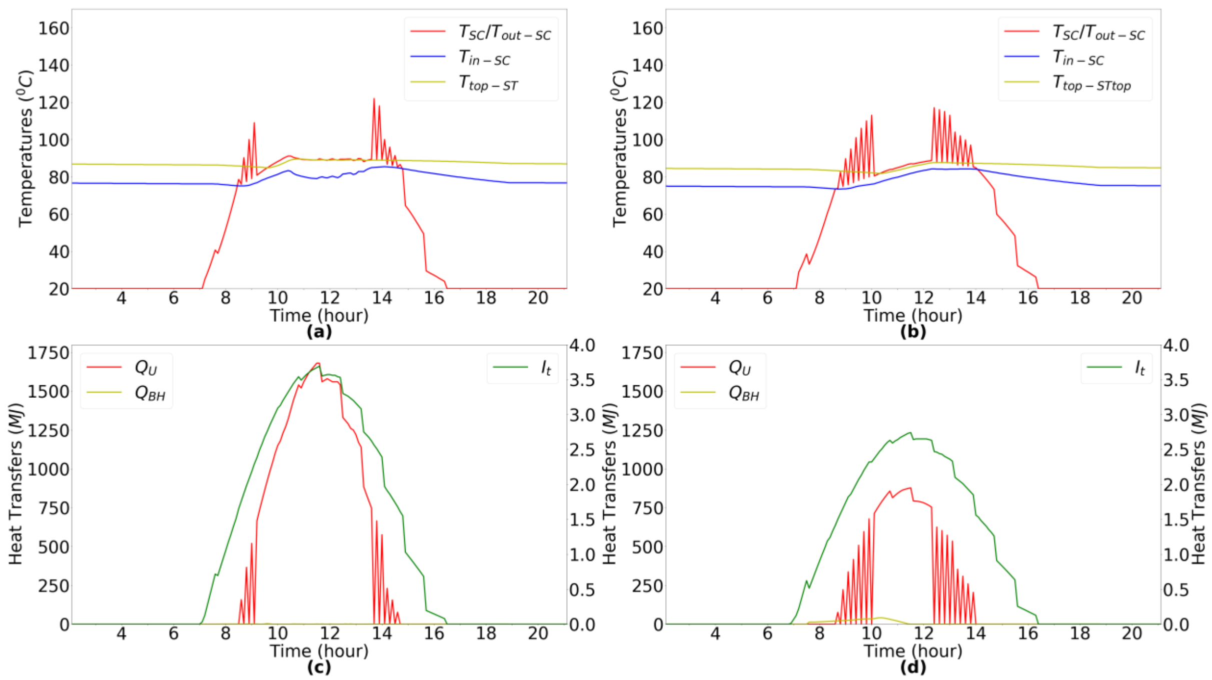

Figure 13: Performance of ULC TRNSYS model in MSD Load 3 (a)&(c) dry, (b)&(d) rainy season

In SLI, a maximum T_{SC} value of 160^0C for the stagnation condition can be reached for Load 1 (Figure 14a) and Load 2 (Figure 15a) in the dry season, while the maximum T_{SC} value of Load 1 (Figure 14b) and Load 2 (Figure 15b) reaches 130^0C in the rainy season. During the dry season, there may be excess solar thermal generation at the peak solar hours for Load 1 and Load 2 (Figures 14c, 15c). During the rainy season, there may be a relatively smaller surplus of solar thermal generation during the peak solar hours (Figures 14d, 15d).

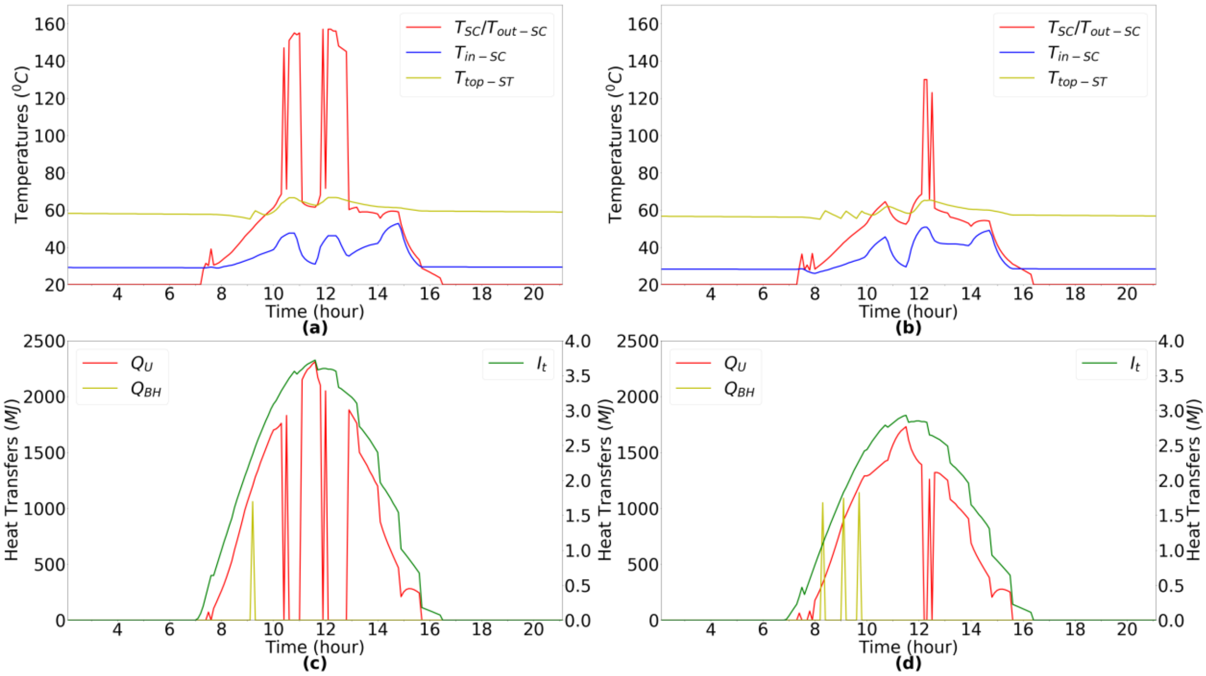

Figure 14: Performance of PLC TRNSYS model in SLI Load 1 (a)&(c) dry, (b)&(d) rainy season

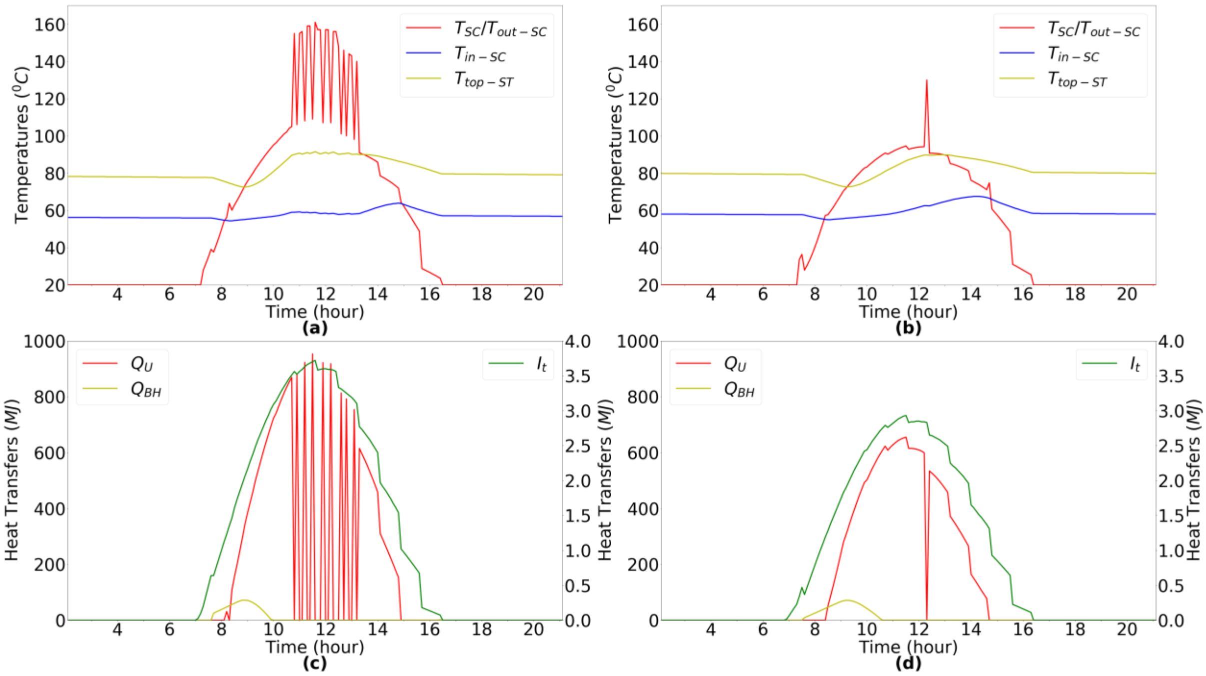

Figure 15: Performance of SLC TRNSYS model in SLI Load 2 (a)&(c) dry, (b)&(d) rainy season

From Figures 11 to 15 (a, b), it can be seen that the temperature variations are closely related to the trend of total irradiance in Figures 11 to 15 (c, d) and to the activity of the control system that controls the recirculation and modulated mass flow in the solar field. By using ST, two main effects can be effectively controlled: limiting the temperature drop due to the cloud effect during the day and increasing the availability of solar heat. This makes the system semi-dispatchable, which in turn allows flexibility in energy generation. These features led to the trends of heat transfer through FPC and BH.

The trend of T_{out_SC} follows almost the same pattern in both processing factories, as the external conditions such as solar radiation and ambient temperature are similar, with relatively low-temperature values during the rainy season. All of these values were comparable to the reported temperatures. FPCs typically operate at temperatures between 85 and 95^{0}C [46][47]. In summer, solar water heating systems often reach stagnation conditions as the ST easily reaches the maximum temperature (≈60-95^{0}C) on a clear day. In this case, the SP is turned off by the C_{SP}. Then, the T_{SC} increases rapidly and reaches the so-called stagnation temperature (≈120-160^{0}C). The stagnation temperature of FPCs with selectively coated absorbers has been reported to be 180 to 210^{0}C [48]. These conditions make this region an acceptable location for FPC installation. In most cases, the T_{out_SC} exceeds the T_{top_ST} margins in both the dry and rainy seasons, making FPC well-suited for use.

For comparison, Figure 16 shows the weekly thermal performance results of the BB for reference and optimal SIH configurations at the MSD. The SF ranges from 80 to 99% for heating and 0 to 35% for cooling in the rainy season and dry season, respectively. This is obviously because the intensity of solar radiation is higher in the dry season than in the rainy season. These results apply equally to both industries and similar applications.

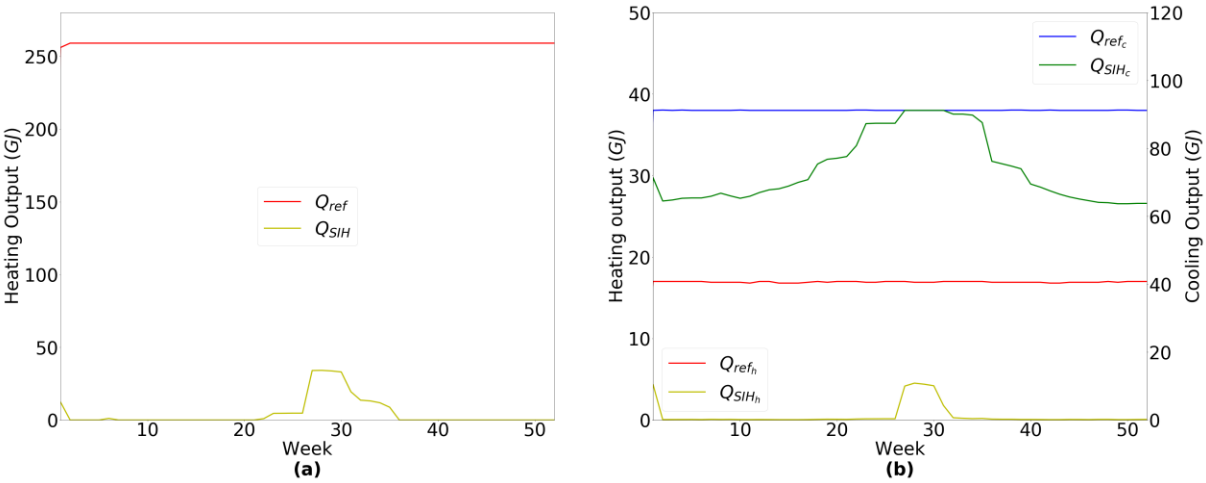

Figure 16: Weekly heat output of the BB and BC at MSD optimal design (a) Load 1 (b) Load 3

Overall, these patterns are beneficial for improving thermal performance by scheduling the delivered energy to allow the system to take advantage of saving maximization. They also help companies make informed decisions about the timing of their needed auxiliary sources.

3.2. Effects of the design parameters on savings and thermal performance

To perform a complete economic study, it is necessary to consider the effects of the design parameters on both cost savings and thermal performance. For evaluation, Figure 17 through Figure 19 show the effects of m_{SC}, A_{SC}, and V_{ST} for MSD configurations. These results apply equally to both industries and similar applications.

From Figure 17a (Load 1) and Figure 17b (Load 3), it can be seen that increasing m_{SC} improves ALCS, SFs, and CE to the optimal point. This is due to the continuous operation of the SP, which lowers the T_{out_SC} and thus maintains the T_{top_ST}. This continuous cooling of the SC extracts more Q_U reduces Q_{BH} and improves CE by reducing convection and radiation losses. However, increasing m_{SC} above the optimal value slowly reduces ALCS, SF, and CE for heating applications (Figure 17a) as T_{out_SC} is further reduced, and the need for Q_{BH} to reach T_{top_ST} increases. At Load 3 (Figure 17b), increasing m_{SC} above the optimal value had little effect on ALCS, while SF_h, SF_c, and CE decreased due to the large m_{SC} at a relatively higher T_{in_SC}, decreasing Q_U and increasing the need for additional Q_{BH} and Q_{BC} to achieve the required setpoint temperatures.

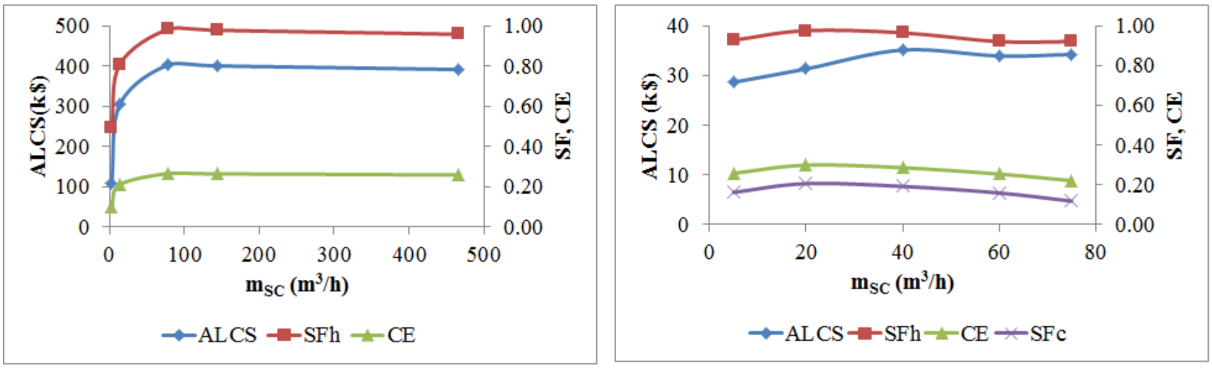

(a) (b)

Figure 17: Effects of m_{SC} on (a) Load 1 and (b) Load 3

From Figure 18a (Load 1) and Figure 18b (Load 3), increasing A_{SC} to the optimal value leads to an improvement in ALCS and SF, mainly because of the increase in T_{out_SC}, which increases T_{top_ST} and decreases the need for Q_{BH} and Q_{BC} to maintain T_{top_ST}. A further increase in A_{SC} forces a decrease in ALCS due to excessive system costs, which also increases T_{out_SC} without improving the need for Q_{BH}. The higher T_{out_SC} leads to a maximum T_{top_ST} at which SP remains off. This turn-off limit reduces the amount of Q_U. For Load 1 (Figure 18a), the increase in A_{SC} above the optimal value at SF was not as pronounced because the optimal design covers almost all of the heating demand. The CE decreases with increasing A_{SC} value, mainly due to lower Q_U and higher heat losses due to convection and conduction at higher T_{SC}. For Load 3 (Figure 168), the increase in A_{SC} value beyond the optimal value was very pronounced for SF_h and SF_c because the optimal design does not cover the entire demand. The increase in CE with increasing A_{SC} is mainly due to higher Q_U and lower heat losses by convection and conduction due to the large mass flow for the water chiller.

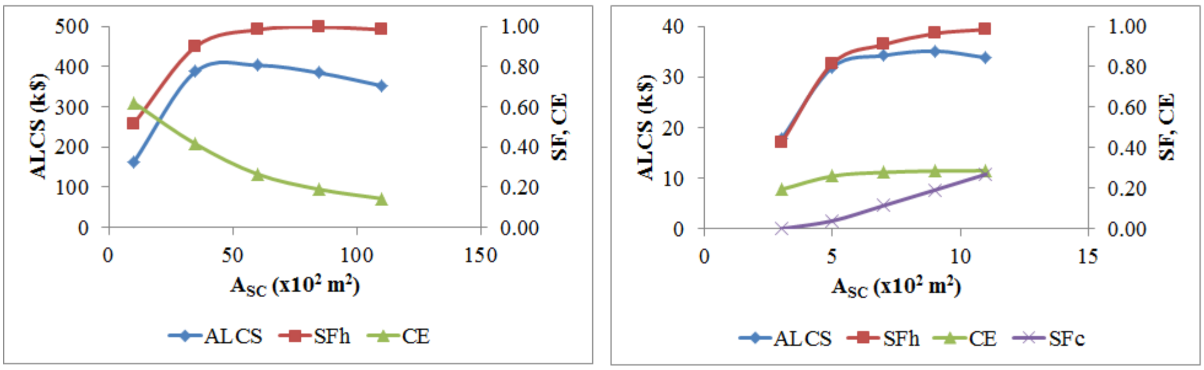

(a) (b)

Figure 18: Effects of A_{coll} on (a) Load 1 and (b) Load 3

From Figure 19a (Load 1) and Figure 19b (Load 3), increasing V_{ST} to the optimum value improves ALCS, SF, SF_h, and CE, mainly due to the high Q_U that keeps the T_{top_ST} below the set point and keeps the SP operating. This provides additional energy savings during periods of high irradiance and reduces the need for Q_{BH}. Increasing V_{ST} above the optimal value results in a decrease in ALCS due to an increase in system capital cost and the need for Q_{BH} to maintain the T_{top_ST} set point. This increase had no impact on SF since the optimal design meets almost all requirements. However, it had little effect on SF_h and SF_c (Figure 19b) because the need for Q_{BH} and Q_{BC} does not improve. Increasing V_{ST} improves CE since increasing V_{ST} lowers the T_{top_ST} and keeps SP running, increasing the amount of Q_U.

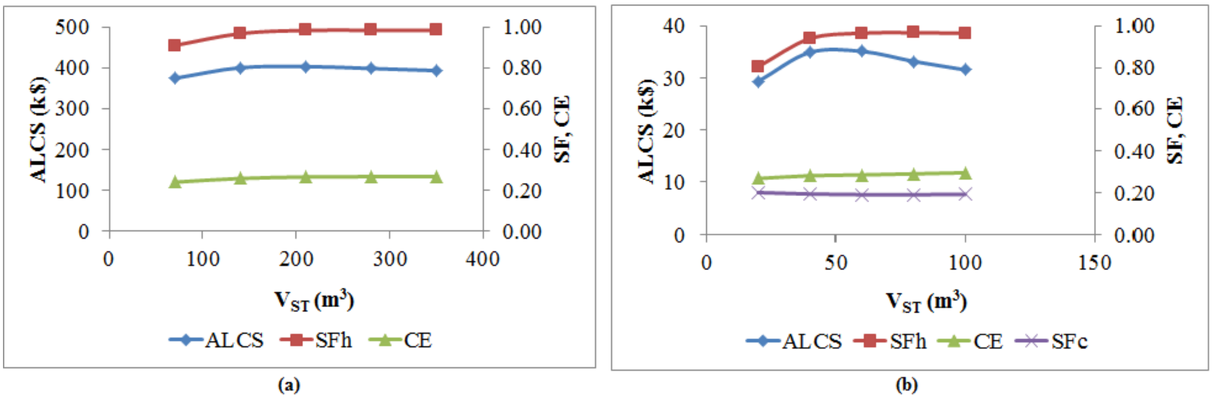

Figure 19: Effects of V_{ST} on (a) Load 1 and (b) Load 3

Overall, large deviations of m_{SC} from optimal values had little effect on ALCS and solar system performance (SF and CE). System cost and efficiency were mainly affected by A_{SC}. V_{ST} was the second largest source of economic and performance impacts. These results are consistent with other relevant findings in the literature. The study by [49] found that solar savings increase with A_{SC} until the optimal value is reached. However, if the A_{SC} is increased further, the fuel savings may continue to increase, and due to the high installation cost, the solar savings decrease. The work in [50][51] has shown that a slight improvement in system performance can be achieved by varying the storage volume.

Since A_{SC} was the parameter with the largest impact, the ALCS, m_{SC}, and V_{ST} values per A_{SC} can be provided for quick estimates (Figure 20 and Figure 21).

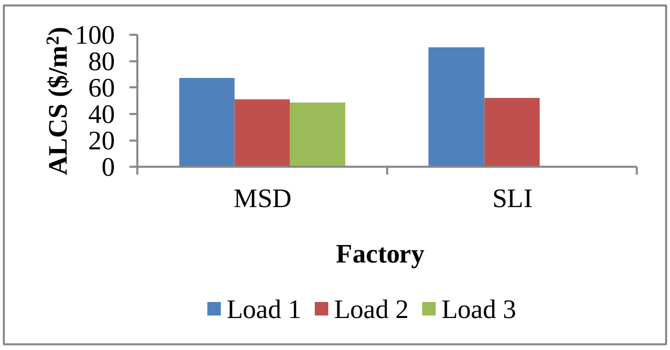

Figure 20: ALCS values per A_{SC}

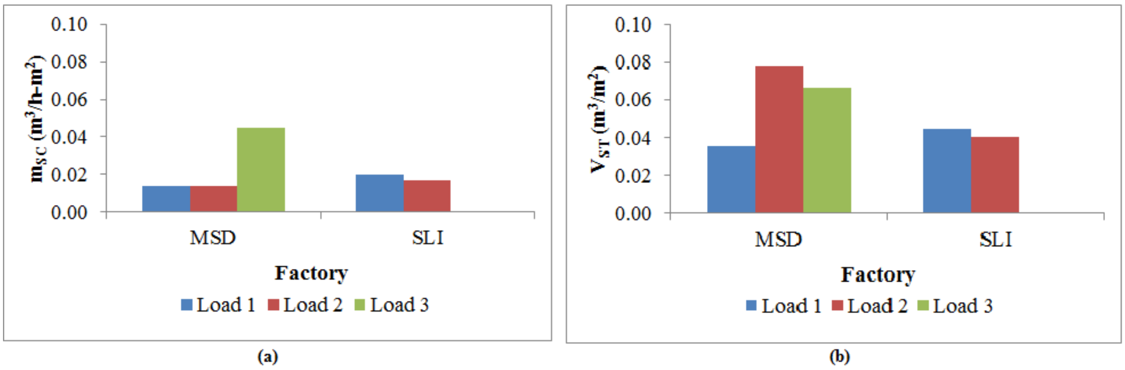

Figure 21: (a) m_{SC} (b) V_{ST} values per A_{SC}

From Figure 20 and Figure 21, the ALCS, m_{SC}, and V_{ST} values per collector area were in the range of \$51-90/m^2, 0.01-0.02m^3/h-m^2, and 0.04-0.08m^3/m^2 for Load 1 and Load 2, respectively, and \$49/m^2, 0.04m^3/h-m^2, and 0.07m^3/m^2 for Load 3. These results agree well with a study by Ferreira et al. [52], who reported 0.07m^3/m^2 as the optimal storage volume per unit area of the solar collector. Based on their study, the relationship between solar energy utilization rate and storage capacity at values higher than 0.09m^3/m^2 does not lead to better utilization of incident solar energy but only increases the storage volume and its cost. Therefore, it can be assumed that Load 1 and Load 2 are the most economical operating concepts that can be replaced by FPC. Load 1 has achieved a higher ALCS per A_{CS}, mainly due to the lower T_{in_SC}. Of the two industries, SLI achieved a higher ALCS per A_{CS} due to the HW withdrawal profile and the low-temperature level required.

4. Conclusions

The study presented a detailed dynamic operation modeling of a SIH system with storage on a systematic control scale. The modeling approach emphasized the statistical optimization based on maximizing the ALCS using TRNSYS. The model was applied to MSD and SLI in Ethiopia. The results showed significant annual savings, acceptable daily performance margins, and a higher impact of collector area on the economic and thermal performance of the optimized system configurations of three operating loads. Annual savings of \$403k, \$23k, and \$35k were obtained for Load 1, Load 2, and Load 3, respectively in MSD, and \$81k and \$26k for Load 1 and Load 2 in SLI. It was observed that the collector started heating at about 7 am, reached the highest temperature at about 12 noon, and dropped at about 6 pm. In the dry season, a maximum collector absorber temperature of 160^{0}C can be reached for the Load 1 and Load 2 configurations, while in the rainy season, the temperature can reach 85 to 130^{0}C. For the Load 3 configuration, a maximum collector absorber temperature of 120^{0}C can be reached in the dry and rainy seasons. Per unit collector area, the annual life-cycle savings, mass flow rate, and storage volume for Load 1 and Load 2 were in the range of \$51-90/m^2, 0.01-0.02m^3/h-m^2, and 0.04-0.08m^3/m^2, respectively. Similarly, the values for Load 3 were \$49/m^2, 0.04m^3/h-m^2, and 0.07m^3/m^2. Thus, the study supports the transient analysis of SIH and provides solutions for the optimal use of solar thermal. The model can then be readily used to estimate and compare other process industries, locations, and technologies. The lesson learned from this study could also help decision-makers understand the options for cost-effective integrations that can make Ethiopia a renewable energy hub, a well-intentioned policy path to pursue in line with the climate-resilient green economy (CRGE) plan of the country.

5. Authors Contributions

Yacob Gebreyohannes: Conceptualization, Methodology, Software, Writing an original draft, Review, and Editing. **Mulu Bayray:** Supervision, Review, and Editing. **Johan Lauwaert:** Supervision, Review, and Editing.

6. Acknowledgment

The authors would like to acknowledge the CoE-REWiSE project at Mekelle University and Global Minds Project at UGent funds for the Ph.D. study leading to this article. We are also grateful for the collaboration of the industries in providing relevant data for the presented analysis.

7. References

[1] Y. Gebreyohannes, M. Bayray, and J. Lauwaert, "A Review on Solar Thermal Utilization for Industrial Heating and Cooling Processes: Global and Ethiopian Perspective," *Momona Ethiopian Journal of Science*, vol. 12, no. 2, pp. 232–256, May 2021, doi: 10.4314/mejs.v12i2.6.

[2] C. A. Schoeneberger, C. A. McMillan, P. Kurup, S. Akar, R. Margolis, and E. Masanet, "Solar for industrial process heat: A review of technologies, analysis approaches, and potential applications in the United States," *Energy*, vol. 206. Elsevier Ltd, p. 118083, Sep. 01, 2020. doi: 10.1016/j.energy.2020.118083.

[3] P. Klein, K. Surridge, and M. Wolf, "Potential of solar heat for industrial processes: a summary of the key findings from Solar Payback," 2018, Accessed: Mar. 17, 2023. [Online]. Available: https://researchspace.csir.co.za/dspace/handle/10204/11012

[4] IEA-ETSAP and IRENA, "Solar heat for industrial processes -Technology Brief," 2015. https://www.ourenergypolicy.org/resources/solar-heat-for-industrial-processes-technology-brief/ (accessed Nov. 05, 2022).

[5] J. Zhang, L. Zhao, S. Deng, W. Xu, and Y. Zhang, "A critical review of the models used to estimate solar radiation," *Renewable and Sustainable Energy Reviews*, vol. 70. Elsevier Ltd, pp. 314–329, Apr. 01, 2017. doi: 10.1016/j.rser.2016.11.124.

[6] P. Gang, L. Guiqiang, Z. Xi, J. Jie, and S. Yuehong, "Experimental study and exergetic analysis of a CPC-type solar water heater system using higher-temperature circulation in winter," *Solar Energy*, vol. 86, no. 5, pp. 1280–1286, May 2012, doi: 10.1016/J.SOLENER.2012.01.019.

[7] S. S. Thabit and J. Stark, "Effects of working patterns on solar generated heat in UK industry," *Appl Energy*, vol. 22, no. 3, pp. 165–186, Jan. 1986, doi: 10.1016/0306-2619(86)90001-2.

[8] Y. G. Hiben, M. B. Kahsay, and J. Lauwaert, "A review on Solar Thermal System Design, Integration, and Technoeconomic Modeling for Industrial Heating and Cooling Processes," in *American Solar Energy Society National Solar Conference 2021 Proceedings, SOLAR 2021*, Dec. 2021, pp. 31–42. doi: 10.18086/solar.2021.01.02.

[9] J. Rawlins and M. Ashcroft, "Small-scale Concentrated Solar Power - A review of current activity and potential to accelerate deployment," *Carbon Trust*, no. March, p. 50, 2013.

[10] P. Kumar *et al.*, "Economics of Implementing Solar Thermal Heating Systems in the Textile Industry," *Energies 2022, Vol. 15, Page 4277*, vol. 15, no. 12, p. 4277, Jun. 2022, doi: 10.3390/EN15124277.

[11] J. L. García, C. J. Porras-Prieto, R. M. Benavente, M. T. Gómez-Villarino, and F. R. Mazarrón, "Profitability of a solar water heating system with evacuated tube collector in the meat industry," *Renew Energy*, vol. 131, pp. 966–976, Feb. 2019, doi: 10.1016/J.RENENE.2018.07.113.

[12] A. A. Ghoneim, "Solar industrial process heat potential in Alexandria, Egypt," *International Journal of Solar Energy*, vol. 11, no. 3–4, pp. 177–184, Jan. 1992, doi: 10.1080/01425919208909737.

[13] M. Siyoum Gudeta, S. Mekbeb, M. Shibeshi, and E. Gardie, "Performance analysis of solar water heater system with heat pipe evacuated tube collector on Moha soft drink industries in Ethiopia," *Case Studies in Thermal Engineering*, p. 102211, Aug. 2022, doi: 10.1016/J.CSITE.2022.102211.

[14] K. Kaci *et al.*, "Design, optimization and economic viability of an industrial low temperature hot water production system in Algeria: A case study," *International Journal of Renewable Energy Development*, vol. 0, no. 0, May 2023, doi: 10.14710/IJRED.2023.49759.

[15] E. C. Joubert, S. Hess, and J. L. Van Niekerk, "Large-scale solar water heating in South Africa: Status, barriers and recommendations," *Renew Energy*, vol. 97, pp. 809–822, Nov. 2016, doi: 10.1016/J.RENENE.2016.06.029.

[16] C. J. Porras-Prieto, F. R. Mazarrón, V. de los Mozos, and J. L. García, "Influence of required tank water temperature on the energy performance and water withdrawal potential of a solar water heating system

equipped with a heat pipe evacuated tube collector," *Solar Energy*, vol. 110, pp. 365–377, Sep. 2014, doi: 10.1016/j.solener.2014.09.030.
[17] F. R. Mazarrón, C. J. Porras-Prieto, J. L. García, and R. M. Benavente, "Feasibility of active solar water heating systems with evacuated tube collector at different operational water temperatures," *Energy Convers Manag*, vol. 113, pp. 16–26, Apr. 2016, doi: 10.1016/J.ENCONMAN.2016.01.046.
[18] R. Silva, M. Berenguel, M. Pérez, and A. Fernández-Garcia, "Thermo-economic design optimization of parabolic trough solar plants for industrial process heat applications with memetic algorithms," *Appl Energy*, vol. 113, pp. 603–614, Jan. 2014, doi: 10.1016/J.APENERGY.2013.08.017.
[19] A. Allouhi *et al.*, "Design optimization of a multi-temperature solar thermal heating system for an industrial process," *Appl Energy*, vol. 206, pp. 382–392, Nov. 2017, doi: 10.1016/J.APENERGY.2017.08.196.
[20] A. Franco, "Methods for the Sustainable Design of Solar Energy Systems for Industrial Process Heat," *Sustainability 2020, Vol. 12, Page 5127*, vol. 12, no. 12, p. 5127, Jun. 2020, doi: 10.3390/SU12125127.
[21] J. D. Gil, A. Topa, J. D. Álvarez, J. L. Torres, and M. Pérez, "A review from design to control of solar systems for supplying heat in industrial process applications," *Renewable and Sustainable Energy Reviews*, vol. 163, p. 112461, Jul. 2022, doi: 10.1016/J.RSER.2022.112461.
[22] J. Immonen and K. M. Powell, "Dynamic optimization with flexible heat integration of a solar parabolic trough collector plant with thermal energy storage used for industrial process heat," *Energy Convers Manag*, vol. 267, p. 115921, Sep. 2022, doi: 10.1016/J.ENCONMAN.2022.115921.
[23] J. A. Duffie and W. A. Beckman, *Solar Engineering of Thermal Processes: Fourth Edition*. John Wiley and Sons, 2013. doi: 10.1002/9781118671603.
[24] "Optimization | SmartUQ." https://www.smartuq.com/software/statistical-optimization/ (accessed Mar. 17, 2023).
[25] G. K. Ijemaru, M. Z. Adamu, E. A. Obatoke, H. Hussaini, and F. O. Ajayi, "Design and Modelling of a Solar Water Heating System," *Industrial Engineering Letters*, vol. 4, no. 12, pp. 70–79, 2014.
[26] World Bank, ESMAP, SOLARGIS, and IFC, "Global Solar Atlas," *Global Solar Atlas*, 2019. https://globalsolaratlas.info/downloads/ethiopia (accessed Apr. 08, 2019).
[27] M. Bayray *et al.*, "Temporal and spatial solar resource variation by analysis of measured irradiance in Geba catchment, North Ethiopia," *Sustainable Energy Technologies and Assessments*, vol. 44, p. 101110, Apr. 2021, doi: 10.1016/j.seta.2021.101110.
[28] "Ethiopia Energy Situation - energypedia." https://energypedia.info/wiki/Ethiopia_Energy_Situation (accessed Oct. 23, 2022).
[29] M. Gebreeyesus, "Industrial Policy and Development in Ethiopia: Evolution and Current Performance," *WIDER Working Paper*, no. 6, 2013.
[30] M. Bayray *et al.*, "Measured solar irradiance data for resource assessment at four sites in Geba catchment, Tigray, North Ethiopia," *Data Brief*, vol. 40, p. 107836, Feb. 2022, doi: 10.1016/J.DIB.2022.107836.
[31] H. Yacob, B. Mulu, and L. Johan, "Assessment of Process Heating and Cooling Potential for Solar System Installation at Typical Industries in Ethiopia," in *EuroSun 2020 Proceedings*, 2021, pp. 1–10. doi: 10.18086/eurosun.2020.03.01.
[32] L. M. Ayompe, A. Duffy, S. J. McCormack, and M. Conlon, "Validated TRNSYS model for forced circulation solar water heating systems with flat plate and heat pipe evacuated tube collectors," *Appl Therm Eng*, vol. 31, no. 8–9, pp. 1536–1542, Jun. 2011, doi: 10.1016/j.applthermaleng.2011.01.046.
[33] T. Osório and M. J. Carvalho, "Testing of solar thermal collectors under transient conditions," *Solar Energy*, vol. 104, pp. 71–81, Jun. 2014, doi: 10.1016/J.SOLENER.2014.01.048.
[34] S. Bahria, M. Amirat, A. Hamidat, M. El Ganaoui, and M. Slimani, "Parametric study of solar heating and cooling systems in different climates of Algeria – A comparison between conventional and high-energy-performance buildings," *Energy*, vol. 113, pp. 521–535, Oct. 2016, doi: 10.1016/J.ENERGY.2016.07.022.
[35] EASE, "Thermal Hot Water Storage," 2016.
[36] International Renewable Energy Agency, "Innovation Outlook: Thermal Energy Storage," 2020.
[37] U.S. DOE, "Combined heat and power technology fact sheet series," 2016.
[38] Broad Air Conditioning Co. Ltd., "Broad XI Non-Electric Chiller Model Selection & Design Manual," 2016.
[39] L. Kumar, M. Hasanuzzaman, and N. A. Rahim, "Global advancement of solar thermal energy technologies for industrial process heat and its future prospects: A review," *Energy Convers Manag*, vol. 195, pp. 885–908, Sep. 2019, doi: 10.1016/J.ENCONMAN.2019.05.081.
[40] M. Krarouch, F. Ruesch, H. Hamdi, A. Outzourhit, and M. Haller, "Dynamic simulation and economic analysis of a combined solar thermal and pellet heating system for domestic hot water production in a traditional Hammam," *Appl Therm Eng*, vol. 180, Nov. 2020, doi: 10.1016/J.APPLTHERMALENG.2020.115839.
[41] "Ethiopia diesel prices, 13-Mar-2023 | GlobalPetrolPrices.com." https://www.globalpetrolprices.com/Ethiopia/diesel_prices/# (accessed Mar. 19, 2023).

[42] "Ethiopia electricity prices, June 2022 | GlobalPetrolPrices.com." https://www.globalpetrolprices.com/Ethiopia/electricity_prices/# (accessed Mar. 19, 2023).
[43] "Inflation rates in Ethiopia." https://www.worlddata.info/africa/ethiopia/inflation-rates.php# (accessed Mar. 19, 2023).
[44] M. T. Boke, S. A. Moges, and Z. A. Dejen, "Optimizing renewable-based energy supply options for power generation in Ethiopia," *PLoS One*, vol. 17, no. 1, p. e0262595, Jan. 2022, doi: 10.1371/JOURNAL.PONE.0262595.
[45] A. K. Sharma, C. Sharma, S. C. Mullick, and T. C. Kandpal, "Solar industrial process heating: A review," *Renewable and Sustainable Energy Reviews*, vol. 78, pp. 124–137, Oct. 2017, doi: 10.1016/J.RSER.2017.04.079.
[46] Z. S. Lu *et al.*, "Study of a novel solar adsorption cooling system and a solar absorption cooling system with new CPC collectors," *Renewable Energy*, vol. 50, pp. 299–306, Feb. 2013, doi: 10.1016/J.RENENE.2012.07.001.
[47] H. L. Luo, R. Z. Wang, Y. J. Dai, J. Y. Wu, J. M. Shen, and B. B. Zhang, "An efficient solar-powered adsorption chiller and its application in low-temperature grain storage," *Solar Energy*, vol. 81, no. 5, pp. 607–613, May 2007, doi: 10.1016/J.SOLENER.2006.09.001.
[48] R. Hausner and C. Fink, "Stagnation behaviour of solar thermal systems A Report of IEA SHC-Task 26 Solar Combisystems Stagnation behaviour of solar thermal systems A technical report of Subtask A * Arbeitsgemeinschaft ERNEUERBARE ENERGIE Institute for Sustainable Technologies A-8200 Gleisdorf, IEA SHC-Task 26-Solar Combisystems," 2002.
[49] J. M. Abdulateef, N. M. Murad, M. A. Alghoul, A. Zaharim, and K. Sopian, "Economic analysis of combined solar-assisted ejector absorption refrigeration system," in *Recent Researches in Geography, Geology, Energy, Environment and Biomedicine - Proc. of the 4th WSEAS Int. Conf. on EMESEG'11, 2nd Int. Conf. on WORLD-GEO'11, 5th Int. Conf. on EDEB'11*, 2011, pp. 157–161.
[50] A. Buonomano, F. Calise, and G. Ferruzzi, "Thermoeconomic analysis of storage systems for solar heating and cooling systems: A comparison between variable-volume and fixed-volume tanks," *Energy (Oxford)*, vol. 59, pp. 600–616, Sep. 2013, doi: 10.1016/J.ENERGY.2013.06.063.
[51] M. C. Rodríguez-Hidalgo, P. A. Rodríguez-Aumente, A. Lecuona, M. Legrand, and R. Ventas, "Domestic hot water consumption vs. solar thermal energy storage: The optimum size of the storage tank," *Appl Energy*, vol. 97, pp. 897–906, 2012, doi: 10.1016/J.APENERGY.2011.12.088.
[52] A. C. Ferreira, A. Silva, J. C. Teixeira, and S. Teixeira, "Multi-Objective Optimization of Solar Thermal Systems Applied to Portuguese Dwellings," *Energies 2020, Vol. 13, Page 6739*, vol. 13, no. 24, p. 6739, Dec. 2020, doi: 10.3390/EN13246739.